

**STUDY OF STRUCTURAL, ELECTRICAL AND MAGNETOELECTRIC  
PROPERTIES OF  $\text{Bi}_{0.9-x}\text{Ca}_{0.1}\text{Y}_x\text{Fe}_{0.9}\text{Zr}_{0.1}\text{O}_3$  CERAMICS**

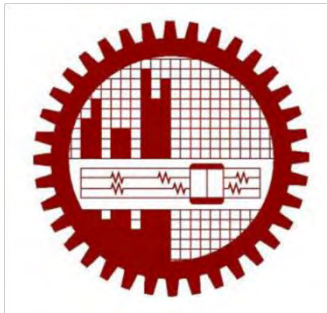
*A dissertation submitted to the Department of Physics, Bangladesh University of Engineering and Technology, Dhaka  
in fulfillment of the requirement for the degree of Master of Philosophy (M. Phil.) in physics*

**by**

**Fatema Tuz Zohora**

**Student No. : 1014143017 F**

**Session : October 2014**



**Department of Physics**

**BANGLADESH UNIVERSITY OF ENGINEERING AND TECHNOLOGY**

**Dhaka-1000, Bangladesh**

**28 September, 2019**

**STUDY OF STRUCTURAL, ELECTRICAL AND MAGNETOELECTRIC  
PROPERTIES OF  $\text{Bi}_{0.9-x}\text{Ca}_{0.1}\text{Y}_x\text{Fe}_{0.9}\text{Zr}_{0.1}\text{O}_3$  CERAMICS**

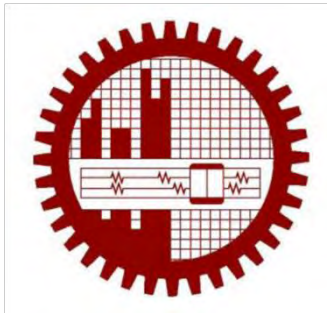
*A dissertation submitted to the Department of Physics, Bangladesh University of Engineering and Technology, Dhaka  
in fulfillment of the requirement for the degree of Master of Philosophy (M. Phil.) in physics*

**by**

**Fatema Tuz Zohora**

**Student No. : 1014143017 F**

**Session : October 2014**



**Department of Physics**

**BANGLADESH UNIVERSITY OF ENGINEERING AND TECHNOLOGY**

**Dhaka-1000, Bangladesh**

**28 September, 2019**

## CANDIDATE'S DECLARATION

*It is hereby declared that this thesis or any part of it has not been submitted elsewhere for the award of any degree or diploma.*

*Fatema Tuz Zohora*

---

FATEMA TUZ ZOHORA

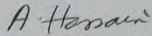
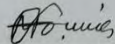

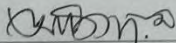
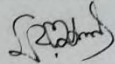
BANGLADESH UNIVERSITY OF ENGINEERING AND TECHNOLOGY (BUET), DHAKA  
DEPARTMENT OF PHYSICS



CERTIFICATION OF THESIS

The thesis titled "STUDY OF STRUCTURAL, ELECTRICAL AND MAGNETOELECTRIC PROPERTIES OF  $\text{Bi}_{0.9-x}\text{Ca}_{0.1}\text{Y}_x\text{Fe}_{0.9}\text{Zr}_{0.1}\text{O}_3$  CERAMICS" submitted by **Fatema Tuz Zohora**, Roll No.1014143017F, Registration No. 1014143017, Session: October/2014, has been accepted as satisfactory in partial fulfillment of the requirement for the degree of **Master of Philosophy** (M. Phil.) on 28 September, 2019.

BOARD OF EXAMINERS

1.   
\_\_\_\_\_  
**Dr. A.K.M. Akther Hossain**  
Professor  
Department of Physics, BUET, Dhaka. Chairman  
(Supervisor)
2.   
\_\_\_\_\_  
**Dr. Md. Forhad Mina**  
Professor and Head  
Department of Physics, BUET, Dhaka. Member  
(Ex-officio)
3.   
\_\_\_\_\_  
**Dr. Md. Mostak Hossain**  
Professor  
Department of Physics, BUET, Dhaka. Member
4.   
\_\_\_\_\_  
**Dr. Mohammad Abu Sayem Karal**  
Associate Professor  
Department of Physics, BUET, Dhaka. Member
5.   
\_\_\_\_\_  
**Dr. Md. Mizanur Rahman**  
Professor  
Department of Physics  
University of Dhaka, Dhaka. Member  
(External)

*Dedicated*

*To*

*My Mother*

***HOSNEARA AKHTER***

*A strong and gentle soul who sacrificed many in life and  
taught me to trust Allah, believe in hard work and that so  
much done in little.*

## *ACKNOWLEDGEMENTS*

*In the name of Allah, the Most Gracious and the Most Merciful.*

*Alhumdulillah, all praises to Allah and His blessing for the completion of this thesis. I thank Allah for all the opportunities, trials and strength that have been showered on me to finish writing the thesis. I experienced so much during this process, not only from the academic aspect but also from the aspect of personality. My humblest gratitude to the holy Prophet Muhammad (Peace be upon him) whose way of life has been a continuous guidance for me.*

*First and foremost, I would like to sincerely thank and express my heartfelt gratitude, indebtedness and profound respect to my supervisor Prof. Dr. A. K. M. Akther Hossain, Department of Physics, BUET for his indispensable guidance, scholastic supervision, patience and generous help throughout the long period of my research works. Most importantly, he has provided positive encouragement and a warm spirit to finish this thesis. It has been a great pleasure and honour to have him as my supervisor.*

*I am extremely grateful to Prof. Dr. Md. Forhad Mina, Head, Department of Physics, BUET for providing the research facilities available in the department during the research work.*

*I would like to thank to the other respectable members of the Doctoral Committee Prof. Dr. Md. Mostak Hossain, Department of Physics, BUET, Prof. Dr. Md. Mizanur Rahman, Department of Physics, University of Dhaka, and Associate Prof. Dr. Mohammad Abu Sayem Karal, Department of Physics, BUET.*

*I would like to express my gratitude to Prof. Dr. Md. Abu Hashan Bhuiyan, Prof. Dr. Jiban Podder, Prof. Dr. Md. Feroz Alam Khan, Prof. Mrs. Fahima Khanam, Prof. Dr. Md. Rafi Uddin, Prof. Dr. Nasreen Akter, Prof. Dr. Mohammed Abdul Basith, Dr. Mohammad Jellur Rahman, Dr. Muhammad Samir Ullah, Dr. Md. Azizar Rahman, Dr. Muhammad Rakibul Islam and all other teachers of Department of Physics, BUET for their sincere cooperation. I would also like to convey my thanks to the employees of the Department of Physics, BUET for their co-operation.*

*I am so thankful to all members of the Solid State Physics Research Laboratory, Department of Physics, BUET for their co-operation and constant support throughout the study.*

*I greatly acknowledge the CASR, BUET to provide financial support for this research. I would like to acknowledge to the authority of the Atomic Energy Center, Dhaka for providing me the facility to perform XRD and M-H hysteresis loop of the studied samples. I also would like to thank to Prof. Dr. Md. Fakhirul Islam, Head, Department of Glass and Ceramic Engineering, BUET for providing me the opportunity to do the SEM and EDX measurements.*

*Finally, I am humbly grateful to my mother, Hosneara Akhter: it is undeniably tough for me to write words that appropriately express my love for you, and my gratitude for all you have gone through in your life for me. I will always remain obligated to you for your unconditional love and support. Your integrity throughout all the aspects and periods of your life has set a standard for me, with which I actively gauge my actions and decisions in life. I'm thankful to my son Muhammad Zarrar Ilan, my brothers S. M. Yousuf Sharif Riyadh and S. M. Rezuanul Rafat and my sister Rabeya Huq Shorna for their patience, love, affection, encouragement and sacrifices during this long period and who have provided me through moral and emotional support in life. I would like to sincerely thank my dearest husband Muhammad Hasan Imam and all other members of my family for their moral support and the sustained inspiration. This dissertation would have never been possible without their care and sacrifices.*

## Abstract

Various multiferroic  $\text{Bi}_{0.9-x}\text{Ca}_{0.1}\text{Y}_x\text{Fe}_{0.9}\text{Zr}_{0.1}\text{O}_3$ , (where,  $x = 0.00$ ,  $x = 0.05$ ,  $x = 0.10$ ,  $x = 0.15$ ,  $x = 0.20$ ) ceramics were synthesized by the standard solid-state reaction technique. The microstructure, dielectric properties, AC conductivity, complex initial permeability, magnetization and magnetoelectric (ME) coefficient of the compositions were investigated. The X-ray diffraction pattern indicated that Yttrium (Y) doped  $\text{BiFeO}_3$  (BFO) ceramics showed a distorted rhombohedral structure. The average grain size was observed to be increased with increasing Y content. The value of dielectric constant ( $\epsilon'$ ) was found decreasing whereas dielectric loss decreasing significantly with increasing of Y content. The  $\text{Bi}_{0.9-x}\text{Ca}_{0.1}\text{Y}_x\text{Fe}_{0.9}\text{Zr}_{0.1}\text{O}_3$ , (where,  $x = 0.20$ ) ceramics had lower value of ( $\epsilon'$ ) than those of  $\text{Bi}_{0.9-x}\text{Ca}_{0.1}\text{Y}_x\text{Fe}_{0.9}\text{Zr}_{0.1}\text{O}_3$ , (where,  $x = 0.00$ ,  $x = 0.05$ ,  $x = 0.10$ ,  $x = 0.15$ ) ceramics. The complex initial permeability was improved with increasing Y concentration and after a certain frequency it was decreases, because of reduced oxygen vacancies which helped to move the domain wall easily. The dielectric and magnetic loss were decreased with the increase of Y content. M-H hysteresis loop was measured for various samples at room temperature and enhanced magnetization was noticed because of the addition of Y in rare earth doped BFO. An enhanced ME coupling was also observed in the studied samples and the highest values of ME coefficient ( $\alpha_{\text{ME}}$ ) was obtained 230 ( $\mu\text{Vcm}^{-1}\text{Oe}^{-1}$ ) for the composition  $x = 0.20$ .



# CONTENTS

	Page No.
<b>Title Page</b>	i
<b>Declaration</b>	ii
<b>Certification</b>	iii
<b>Dedication</b>	iv
<b>Acknowledgements</b>	v
<b>Abstract</b>	vii
<b>Contents</b>	viii
<b>List of symbols</b>	xiii

## **CHAPTER 1 INTRODUCTION AND REVIEW WORKS**

<b>1.1</b>	<b>Introduction and Review Works</b>	01
<b>1.2</b>	<b>Objectives of the present work</b>	03
<b>1.3</b>	<b>Review of the earlier works</b>	04
	References	07

## **CHAPTER 2 THEORITICAL BACKGROUND**

<b>2.1</b>	<b>Multiferroics</b>	09
	2.1.1 Classifications of multiferroics	10
	2.1.2 Magnetoelectric effect	11
<b>2.2</b>	<b>Perovskite structure</b>	12
<b>2.3</b>	<b>Dielectrics</b>	13

2.3.1	Electric polarization	15
2.3.2	Mechanism of polarization	15
2.3.2.1	Space charge /interfacial polarization	16
2.3.2.2	Dipolar or orientation polarization	16
2.3.2.3	Ionic polarization	16
2.3.2.4	Electronic polarization	17
2.3.3	Dielectric properties	18
2.3.3.1	Dielectric constant	18
2.3.3.2	Dielectric loss	19
2.3.4	Dependence of dielectric properties	21
2.3.4.1	Dependence of dielectric constant on frequency	21
2.3.6	Jonscher's power law	22
<b>2.4</b>	<b>Magnetization</b>	<b>23</b>
2.4.1	Ferro-, antiferro- and ferri- magnetic properties	24
2.4.2	Magnetic exchange interaction	24
2.4.2.1	Direct exchange interaction	25
2.4.2.2	Superexchange interaction	26
2.4.2.3	Dzyaloshinskii-Moriya (DM) interaction	27
2.4.3	Theories of permeability	29
<b>2.5</b>	<b>Multiferroic material BiFeO<sub>3</sub></b>	<b>31</b>
	References	33

## CHAPTER 3

### SAMPLE PREPARATION AND EXPERIMENTAL TECHNIQUES

<b>3.1</b>	<b>Introduction</b>	<b>35</b>
3.1.1	Standard solid state reaction technique	35
3.1.2	Synthesis of samples for the present research	36
3.1.3	Calcination schedule	37
3.1.4	Sintering	38
3.1.5	The stages in preparation of sample	39
3.1.6	Preparation of samples for the present research	40
<b>3.2</b>	<b>Characterization techniques</b>	<b>41</b>
3.2.1	X-ray diffraction	42
3.2.2	Scanning electron microscopy	43
3.2.3	Energy dispersive X-ray spectroscopy	44
3.2.4	Dielectric measurements	45
3.2.5	Complex impedance spectroscopy analysis	46
3.2.6	Magnetic properties	46
3.2.6.1	M-H hysteresis loops	47
3.2.6.2	Complex initial permeability	48
3.2.7	Magnetoelectric coefficient	48
	References	49

## CHAPTER 4

### RESULTS AND DISCUSSION

<b>4.1</b>	<b>X- ray diffraction analysis</b>	<b>51</b>
<b>4.2</b>	<b>Density and Porosity</b>	<b>52</b>
<b>4.3</b>	<b>Microstructural analysis</b>	<b>54</b>
<b>4.4</b>	<b>Energy dispersive X-ray spectroscopy analysis</b>	<b>58</b>
<b>4.5</b>	<b>Dielectric properties</b>	<b>61</b>
4.5.1	Real part of dielectric constant	61
4.5.2	Imaginary part of dielectric constant	62
4.5.3	Dielectric loss	63
<b>4.6</b>	<b>The AC conductivity</b>	<b>64</b>
<b>4.7</b>	<b>Magnetic Properties</b>	<b>66</b>
4.7.1	Real part of complex permeability	66
4.7.2	Imaginary part of complex permeability	69
4.7.3	Magnetic loss	71
4.7.4	RQF	73
<b>4.8</b>	<b>Magnetization</b>	<b>76</b>
	M-H hysteresis loops	77
<b>4.9</b>	<b>Magnetoelectric properties</b>	<b>78</b>
	References	81

**CHAPTER 5**  
**CONCLUSIONS**

<b>5.1</b>		84	
	5.1	<b>Conclusions</b>	85

## ABBREVIATIONS OF SYMBOLS AND TERMS

ME	Magnetolectric
PT	PbTiO <sub>3</sub>
BFO	BiFeO <sub>3</sub>
$\mu_B$	Bohr magneton
$\mu_{eff}$	Effective magnetic moment
XRD	X-ray Diffraction
FESEM	Field Emission Scanning Electron Microscope
$\epsilon'$	Dielectric constant
$\epsilon_o$	Permittivity in free space/vacuum
$\tan \delta_E$	Dielectric loss
$\sigma_{AC}$	AC conductivity
$\sigma_{dc}$	dc conductivity
s	Frequency exponent
$\alpha_{ME}$	Magnetolectric coefficient
T <sub>c</sub>	Curie temperature
T <sub>N</sub>	Néel temperature
t	Tolerance factor
$\bar{E}$	Electric field
$\bar{P}$	Polarization
E <sub>c</sub>	Coercive electric field
P <sub>r</sub>	Remnant polarization
$\bar{p}$	Electric dipole moment

$\bar{D}$	Electric displacement
C	Capacitance with dielectric
$C_0$	Capacitance in free space
d	Thickness
$\omega$	Angular frequency
$\tau_0$	Relaxation time
M	Magnetization
H	Magnetic field
DM	Dzyaloshinskii-Moriya
$M_r$	Remnant magnetization
$M_s$	Saturation magnetization
$H_c$	Coercivity
$\mu_i$	Complex initial permeability
$\mu_i'$	Real part of complex initial permeability
$\mu_i''$	Imaginary part of complex initial permeability
$\tan \delta_M$	Magnetic loss
$\rho_x$	X-ray density
$\rho_B$	Bulk density
EDX	Energy Dispersive X-ray Spectroscopy
D	Average value of grain size

## CHAPTER 1

### INTRODUCTION AND REVIEW WORKS

#### 1.1 Introduction

The term multiferroic was first used by H. Schmid in 1994 [1]. Multiferroic materials (MFMs) that exhibit more than one ferroic orders such as ferromagnetic and ferroelectric orders in the same phase have great attention in recent years and are used in various practical devices. Multiferroics have immense application in data storage, spin valves, spintronics, quantum electromagnets and microelectronic devices etc. Multiferroics are very rare in nature because the criteria for being simultaneously ferroelectric and ferro/antiferromagnetic are mutually restricted. Only a small group of compounds can exhibit both magnetic and electric order parameters simultaneously. In these selected materials, magnetic field can not only control magnetization but also induce ferroelectricity or electric field can reorient polarization as well as spin directions. This functionality offers an extra degree of freedom and provides the possibility to create new devices based on these materials. In the most general sense the field of multiferroics was born from studies of magnetoelectric (ME) systems [2]. The ME effect was first observed by Rontgen in 1888 [3] and by Pierre Curie in 1894 [4] in two independent studies. Rontgen found that a dielectric when moved in an electric field, became magnetized and conversely it became polarized when moved in a magnetic field. In contrast, Curie pointed out the ME effect based on symmetry considerations. Simultaneous onset of ferroelectricity and ferromagnetism (of the weak type) was observed to be occurred in nickel iodine boracite  $\text{Ni}_3\text{B}_7\text{O}_{13}\text{I}$  (below about 334 °C) [5]. Mutiferroic properties having perovskite structure was experimentally first observed by Kimura et al. [7] and Wang et al. in 2003 [8].

Ceramics are defined as the solid compounds that consist of metallic and nonmetallic elemental solids which are formed by the application of heat and /or pressure [9]. In general,



ceramic materials have high dielectric strength and high dielectric constant. The properties of ceramic materials depend on the types of atoms present, the nature of bonding between the atoms and the way the atoms are packed together. The atoms in ceramic materials are held together by a chemical bond. Two most common chemical bonds for ceramic materials are covalent and ionic bonding. In comparison to metals, ceramics have very low electrical conductivity due to ionic-covalent bonding which does not form free electrons. Most of the ceramic materials are dielectrics which possess very low electrical conductivity but supports electrostatic field. Electrical conductivity of ceramics varies with the frequency of the applied field and also with temperature [10].

The dielectrics are electrical insulating materials, which can be polarized by the application of electric field. All the dielectrics are insulators but all the insulators are not dielectrics. Dielectrics are classified into non-polar and polar types. When an electric field is applied to dielectric materials, displacement of center of positive and center of negative charge occurs, which creates a dipole moment. By this way dielectric materials store energy. The elementary dipoles in the dielectric materials interact with each other under certain thermodynamic conditions. The internal electric field produced by the interaction of dipoles aligns the dipoles in the same direction. This gives rise the spontaneous polarization in the dielectric material. The polar dielectric materials with spontaneous polarization even in the absence of externally applied electric field are called as ferroelectric materials [11]. Most of the ceramics exhibit ferroelectric behavior. Ferroelectric materials are a subgroup of pyroelectric materials in which polarization can be reversed or reoriented by applying a reverse electric field. Most important property of ferroelectric materials is the formation of hysteresis loop due to its polarization reversal property. Upto certain electric field the ferroelectric material shows the linear relationship between electric field ( $\bar{E}$ ) and polarization ( $\bar{P}$ ). At relatively high  $\bar{E}$ ,  $\bar{P}$  shows a nonlinear relationship with the field.

Amongst the multiferroic materials, BiFeO<sub>3</sub> (BFO) exhibit multiferroic properties at and above room temperature [5-9]. BFO having perovskite ABO<sub>3</sub> (A=Bi, B=Fe) structure, exhibit ferroelectric (T<sub>C</sub>~1103K) and anti-ferromagnetic (T<sub>N</sub>~643K) properties [4]. However, pure phase of BFO is difficult to obtain [10, 11] and various impurity phases (e.g. Bi<sub>2</sub>Fe<sub>4</sub>O<sub>9</sub>, Bi<sub>36</sub>Fe<sub>24</sub>O<sub>57</sub> and Bi<sub>25</sub>FeO<sub>40</sub>) have been reported [12]. The magnetic structure of BFO arising from the Dzyaloshinskii–Moriya interaction give rise to weak ferromagnetism in BFO [13]. It has been reported that rare earth elements such as La [13, 14] and Dy [15] substitution can suppress the spin cycloid structure in BFO and therefore enhancing the magnetic properties. The Y<sup>3+</sup> (radius=2.32 Å), which has an electronic configuration closer to that of La<sup>3+</sup> (radius=2.43 Å) but an ionic radius comparable to Dy<sup>3+</sup> (radius=2.31 Å), seems to be an interesting candidate for the enhancement of multiferroic properties of BFO [16]. A-site and B-site co-doping is a good way to improve the multiferroic properties of BFO, both in films and ceramics [16, 17]. A-site (Bi-site) substitution by Ca<sup>2+</sup> ions and B-site (Fe-site) by Zr<sup>4+</sup> ions improved the multiferroic properties of BFO was reported by different authors [18, 19]. Considering the above facts, Bi<sub>0.9-x</sub>Ca<sub>0.1</sub>Y<sub>x</sub>Fe<sub>0.9</sub>Zr<sub>0.1</sub>O<sub>3</sub> compositions are chosen for this research.

## 1.2 Objectives of the present work

*The main objectives of the proposed research are as follows:*

- Preparation of various Bi<sub>0.9-x</sub>Ca<sub>0.1</sub>Y<sub>x</sub>Fe<sub>0.9</sub>Zr<sub>0.1</sub>O<sub>3</sub> (with x=0, 0.05, 0.10, 0.15, 0.20) MFMs.
- Study of crystal structure and hence determination of lattice parameters, density and porosity of various compositions.
- Investigation of surface morphology and compositional analysis.
- Measurement of complex initial permeability, loss tangent and relative quality factor.

- Investigation of dielectric properties (dielectric constant and dielectric loss), AC conductivity.
- Investigation of DC magnetization.
- Investigation of ME effect as a function of magnetic field.

### 1.3 Review Works

At the first half of the twentieth century several major studies have been done by different researchers in different parts of the world for the development of magnetic materials began in Japan by researchers V. Kato, T. Takei, N. Kawai in the 1930 and by J. Snoek of the Philips Research Laboratories in the period 1935-45 in Netherlands. By Snock in 1945 had laid down the basic fundamentals of the physics and technology of practical ferrite materials. In 1948, the Neel theory of ferromagnetic provided the theoretical understanding of this type magnetic [23]. A. Gautam et al.[21] synthesized Y doped BiFeO<sub>3</sub> polycrystalline ceramics by sol gel method. Crystal structure examined by X-ray diffraction (XRD) indicates that the samples were single phase and crystallize in rhombohedral structure. An anomaly in the dielectric constant and dielectric loss in the vicinity of the antiferromagnetic Neel temperature (TN) was observed. Saturated magnetization loops were observed for all samples with saturated magnetization  $M_s=0.678$  emu/g and remnant magnetization  $M_r=0.084$  emu/g for  $x=0.3$ . There is strong evidence that both lattice constants  $a$  and  $c$  of the unit cell unusually change at Y content of about  $x = 0.10$  [23]. The effect of introducing  $Y^{3+}$  is shown to increase the optical band gap for doped sample Bi<sub>1-x</sub>Y<sub>x</sub>FeO<sub>3</sub> [20, 23]. Additionally, the Raman measurement performed for the lattice dynamics study of Bi<sub>1-x</sub>Y<sub>x</sub>FeO<sub>3</sub> samples reveals a strong band centered at around 1150–1350cm<sup>-1</sup> which is associated with the resonant enhancement of two-phonon Raman scattering in the multiferroic Bi<sub>1-x</sub>Y<sub>x</sub>FeO<sub>3</sub> samples.

The impedance spectroscopy indicates that, the Y dopant has improved the grain impedance. The enhancement of magnetization was observed in Y-doped samples compared to pure  $\text{BiFeO}_3$ . V. Singh et al [33] synthesized  $\text{Bi}_{1-x}\text{Y}_x\text{FeO}_3$  ceramics with compositions  $x=0.00, 0.05, 0.10, 0.15$  and  $0.20$  by the solid state reaction route. All the compositions have shown single phase formation with minor impurities. Microstructural studies reveal that  $\text{Y}^{3+}$  substitution influences grain growth, which in turn affects the dielectric and optical properties of these materials. Dielectric anomalies in temperature dependent dielectric plots at around the magnetic transition temperature (TN) indicate magneto-electric coupling. AC conductivity has been found to decrease with increasing  $\text{Y}^{3+}$  concentration. M. Luo et al. [35] synthesized powder samples of  $\text{Bi}_{1-x}\text{Y}_x\text{FeO}_3$  (BFO,  $x=0, 0.02, 0.05$  and  $0.1$ ) by sol-gel method in this paper. The BFO is crystallized in rhombohedrally distorted perovskite structure with space group R3c. Y doping generates structural evolution in BFO toward orthorhombic Pnma structure due to the adequate substitution of  $\text{Bi}^{3+}$ . In 12–18 GHz, both the dielectric constant and the loss tangent increase with Y-doping, but a compositional independent dielectric loss peak is observed at about 15.5 GHz. The leakage loss is reduced due to the decrease of oxygen vacancies. Main contribution of the dielectric loss is ascribed to dipole polarization. During the doping process, the improved prevention of leakage current enhances the polarization of BFO samples where as the magnetism is enhanced by the suppression of the long-range spiral spin modulation. L. Luo et al. [36] synthesized  $\text{Bi}_{1.04-x}\text{Y}_x\text{FeO}_3$  ceramics with  $x$  up to 0.30 by a tartaric acid modified sol-gel method. The crystal structure transformed from rhombohedral (R3c) to orthorhombic (Pn21a) with increasing Y doping concentration, which was confirmed by the X ray diffraction (XRD) and Raman measurements. With increasing Y doping concentration  $x$ , the leakage current was effectively suppressed, and the room temperature ferromagnetism was strongly enhanced with increasing  $x$  to 0.30. Clear room temperature ferromagnetism with saturate magnetization of about 0.31

emu/g and ferroelectric properties with  $251 \text{ C/cm}^2$  under electric field of  $120 \text{ kV/cm}$  have been observed in orthorhombic  $\text{Bi}_{0.74}\text{Y}_{0.30}\text{FeO}_3$ , suggesting the potential multiferroic applications.

## References

- [1] Schmid, H., "Multi-ferroic magnetoelectric", *Ferroelectrics*, Vol. 162, pp. 317- 338, 1994.
- [2] Smolenskii, G. A. and Chupis, I. E., "Ferroelectromagnets", *Sov. Phys. Usp.*, Vol. 25, pp. 475-493, 1982.
- [3] Röntgen, W. C., "Description of the apparatus with which the experiments on the electro dynamic effect of moving dielectric were performed", *Ann. Phys.*, Vol. 35, pp. 264-283, 1888.
- [4] Curie, P., *J. Phys. (3rd Series)*, Vol. 3, pp. 393, 1894.
- [5] Ascher, E., Rieder, H., Schmid, H. and Stossel, H., "Some properties of ferromagnetoelectric Nickel-Iodine Boracite,  $\text{Ni}_3\text{B}_7\text{O}_{13}\text{I}$ ", *J. Appl. Phys.*, Vol. 37, pp. 1404-1405, 1966.
- [6] Smolensky, G. A. and Ioffe, V. A., International Symposium/Magnetism Grenoble, Communication No. 71, 1958.
- [7] Kimura, T., Goto, T., Shintani, H., Ishizaka, K., Arima, T. and Tokura, Y., "Magnetic control of ferroelectric polarization", *Nature*, Vol. 426, pp. 55-58, 2003.
- [8] Wang, J., Neaton, J. B., Zheng, H., Nagarajan, V., Ogale, S. B., Liu, B., Viehland, D., Vaithyanathan, V., Schlom, D. G., Waghmare, U. V., Spaldin, N. A., Rabe, K. M., Wuttig, M. and Ramesh, R., "Epitaxial  $\text{BiFeO}_3$  multiferroic thin film heterostructures", *Science*, Vol. 299, pp. 1719-1722, 2003.
- [9] Barsoum, M. W., "Fundamental of ceramics", *Taylor and Francis*, 2003.
- [10] Jonscher, A. K., "Dielectric relaxation in solids", *J. Phys. D: Appl. Phys.*, Vol. 32, pp. 57-70, 1999.
- [11] Xu, Y., "Ferroelectric materials and their applications", North-Holland Elsevier Sci. Publ., Amsterdam, 1991.
- [12] Takenaka, T., "Piezoelectric properties of some lead-free ferroelectric ceramics", *Ferroelectrics*, Vol. 230, pp. 87-98, 1999.
- [13] Royan, P. and Swars, K., "The system of bismuth ferric oxide in the range from 0 to 55 mol-percent iron oxide", *Angewandte chemie*, Vol. 69, pp. 779-784, 1957.
- [14] Moreau, J., Michel, C., Gerson, R. and James, W., "Ferroelectric  $\text{BiFeO}_3$  X-ray and neutron diffraction study", *J. Phys. Chem. Solids*, Vol. 32, pp. 1315-1320, 1971.
- [15] Cai, W., Zhong, S., Fu, C., Chen, G. and Deng, X., "Microstructure, dielectric and ferroelectric properties of  $x\text{BaZr}_{0.2}\text{Ti}_{0.8}\text{O}_3-(1-x)\text{BiFeO}_3$  solid solution ceramics", *Mater. Res. Bull.*, Vol. 50, pp. 259-267, 2014.
- [16] Sunder, V., Halliyal, A. and Umarji, A. M., "Investigation of tetragonal distortion in the  $\text{PbTiO}_3$ - $\text{BiFeO}_3$  system by high-temperature X-ray diffraction", *J. Mater. Res.*, Vol. 10, pp. 1301-1306, 1995.
- [17] Shariq, M., Kaur, D. and Chandel, V. S., "Investigation of structural and magnetic properties of Pb free multiferroic  $(\text{BiFeO}_3)_{(1-x)}-(\text{BaTiO}_3)_x$  solid solutions", *AIP Conf. Proc.*, Vol. 1742, pp. 030018, 2016.
- [18] Smith, R. T., Achenbach, F. D., Gerson, R. and James, W. J., "Dielectric properties of solid solutions of  $\text{BiFeO}_3$  with  $\text{Pb}(\text{Ti}, \text{Zr})\text{O}_3$  at high temperature and high frequency", *J. Appl. Phys.*, Vol. 39, pp. 70-74, 1968.
- [19] Kumer, M., Srinivas, A., Suryanarayana, S. V. and Bhimasankaram, T., "Dielectric and impedance studies on  $\text{BiFeO}_3$ - $\text{BaTiO}_3$  solid solutions", *Phys. Status Solidi A*, Vol. 165, pp. 317-326, 1998.

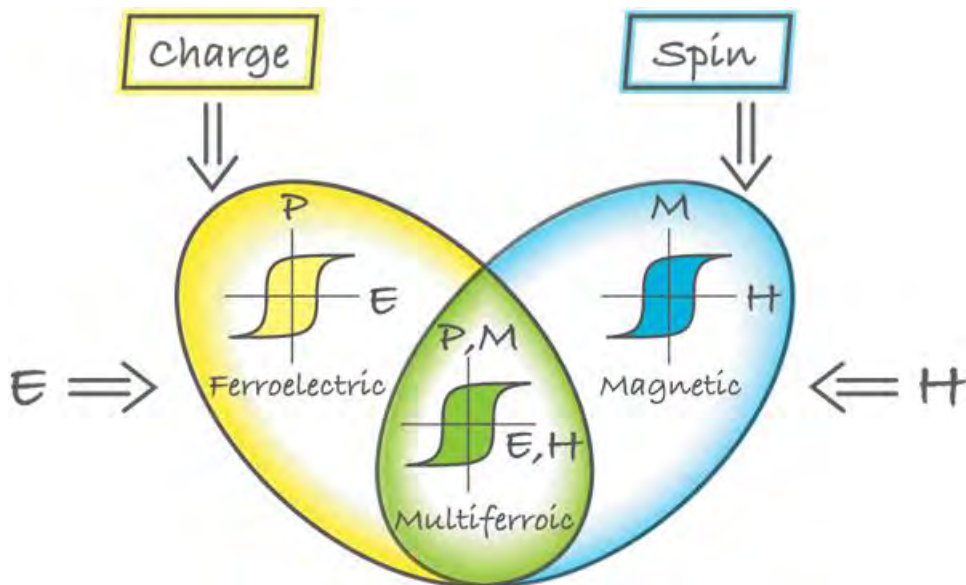
- [20] Chandarak, S., Unruan, M., Sareein, T., Ngamjarurojana, A., Maensiri, S., Laoratanakul, P., Ananta, S. and Yimnirun, R., “Fabrication and characterization of  $(1-x)\text{BiFeO}_3-x\text{BaTiO}_3$  ceramics prepared by a solid state reaction method”, *J. Mater.*, Vol. 14, pp. 120-123, 2009.
- [21] Kumar, M. M., Srinivas, A., Kumar, G. S. and Suryanarayana, S. V., “Investigation of the magnetoelectric effect in  $\text{BiFeO}_3\text{-BaTiO}_3$  solid solutions”, *J. Phys.: Cond. Matt.*, Vol. 11, pp. 8131–8139, 1999.
- [22] Kumar, M. M., Srinivas, A., Suryanarayana, S. V., Kumar G. S. and Bhimasankaram, T., “An experimental setup for dynamic measurement of magnetoelectric effect”, *Bull. Mater. Sci.*, Vol. 21, pp. 251–255, 1998.
- [23] Gotardo, R. A. M., Viana, D. S. F., Dionysio, M. O., Souza, S. D., Garcia, D., Eiras, J. A., Alves, M. F. S., Cotica, L. F., Santos, I. A. and Coelho, A. A., “Ferroic states and phase coexistence in  $\text{BiFeO}_3\text{-BaTiO}_3$  solid solutions”, *J. Appl. Phys.*, Vol. 112, pp. 104112-104115, 2012.

## CHAPTER 2

### THEORITICAL BACKGROUND

#### 2.1 Multiferroics

The coupling between two or more ferroic orders such as ferroelectric, ferromagnetic/antiferromagnetic, ferroelastic etc. is called magnetoelectric coupling. Materials exhibit the coupling is known as multiferroic materials or simply multiferroics (as in Fig. 2.1). According to H. Schmid [1], “Crystals can be defined as multiferroic when two or more of the primary ferroic properties are united in the same phase”. Research on multiferroics is going on since early 1950 although all the effort was theoretical. After an initial burst of interest, research remained static until early 2000. Three major experimental breakthrough in multiferroic research occurred in 2003-04: the discovery of enhanced magnetoelectric coupling in thin films of  $\text{BiFeO}_3$  by Wang et al. [2], the magnetic control of electric polarization in  $\text{TbMnO}_3$  by Kimura et al. [3] and in  $\text{TbMn}_2\text{O}_5$  by Hur et al. [4]. Since then, several new multiferroic materials have been discovered and studied.



**Fig. 2.1** Schematiillustration of multiferroic materials [5].



There are significant scientific and technological interests in multiferroics due to their unusual response, including very large magnetoelectric susceptibility, giant magnetostriction and ME coupling coefficients. In addition, the ability to make coupling between the spontaneous orders parameters offers extra degrees of freedom in the design of conventional devices.

### 2.1.1 Grouping of multiferroics

Multiferroic materials can broadly be classified in two categories namely single phase multiferroic and composite multiferroic. Single phase multiferroic materials show both ferroelectric and ferromagnetic order and they have similar crystal structure. For the case of single phase multiferroic, multiferroicity is intrinsic effect of the material. Multiferroicity in composite materials results from the combination of two materials those are ferroelectric and ferromagnetic separately. For the case of composite multiferroic, multiferroic order is not intrinsic and they have different structures. The scarcity of single phase multiferroic materials makes composite materials an interesting alternative.

Single-phase multiferroics can be further classified into two groups:

- a) Type-I multiferroics
- b) Type-II multiferroics

Type-I multiferroics are those materials in which ferroelectricity and ferromagnetism have different sources and appear largely independently of one another, though there is some coupling between them. In these materials, ferroelectricity typically appears at higher temperatures than magnetism and the spontaneous polarization is often rather large. Example of type-I multiferroic is  $\text{BiFeO}_3$ .

Type-II multiferroic is a novel class of multiferroics in which ferroelectricity exists only in a magnetically ordered state and is caused by a particular type of magnetism. Moreover,

very strong coupling between ferroelectric and magnetic order parameters has also been observed. Magnetic spin structure in type-II multiferroics can be either a spiraling cycloid type or a collinear type.  $\text{TbMnO}_3$ ,  $\text{HbMnO}_3$  etc. are the examples of type-II multiferroic.

### 2.1.2 Magnetoelectric effect (ME)

Magnetoelectric (ME) effect is an important phenomenon for multiferroic materials. The induction of electric polarization by means of a magnetic field and the induction of magnetization by means of an electric field is defined as the ME effect (Fig. 2.2). The ME effect was theoretically explained by Dzyaloshinskii [6] with a prediction being made for  $\text{Cr}_2\text{O}_3$  that was verified experimentally in this compound by Astrov [7] in late 1950s. After several years, the ME effect was observed in boracites materials ( $\text{Ni}_3\text{B}_7\text{O}_{13}\text{I}$ ) by Schmid [1]. ME effect in perovskite compound BFO was first observed by Smolenskii and Chupis [8]. The ME effects can be linear or/and non-linear with respect to the external electric field or magnetic field.

The ME effect is observed both in single phase and composite multiferroics. The P-E

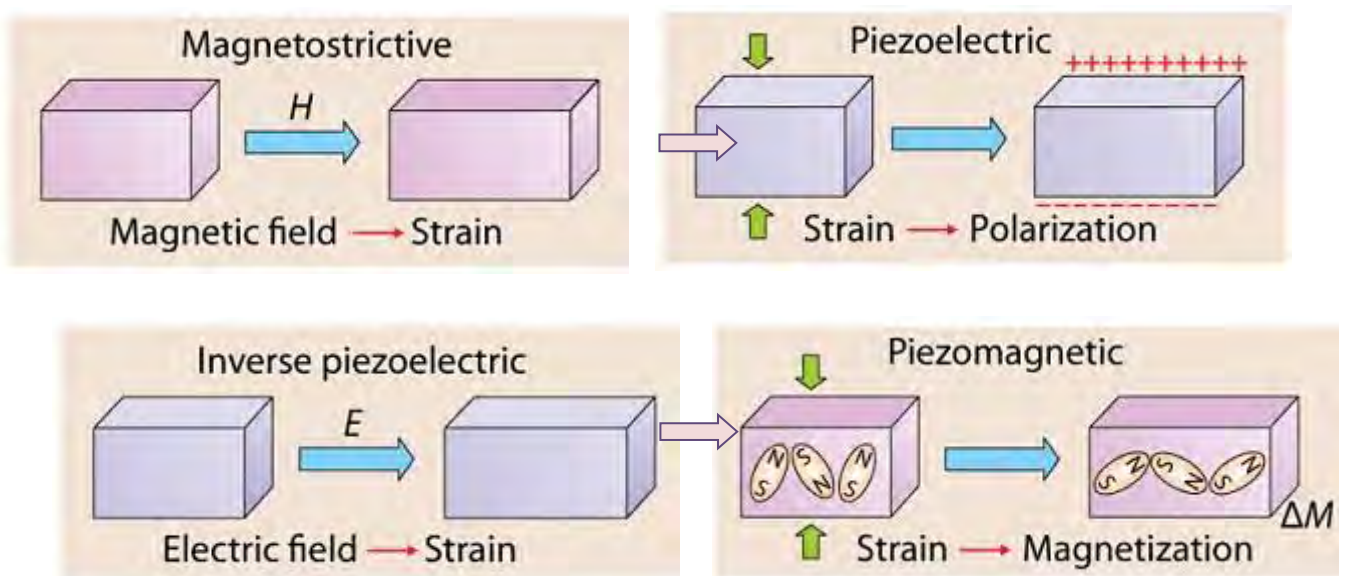
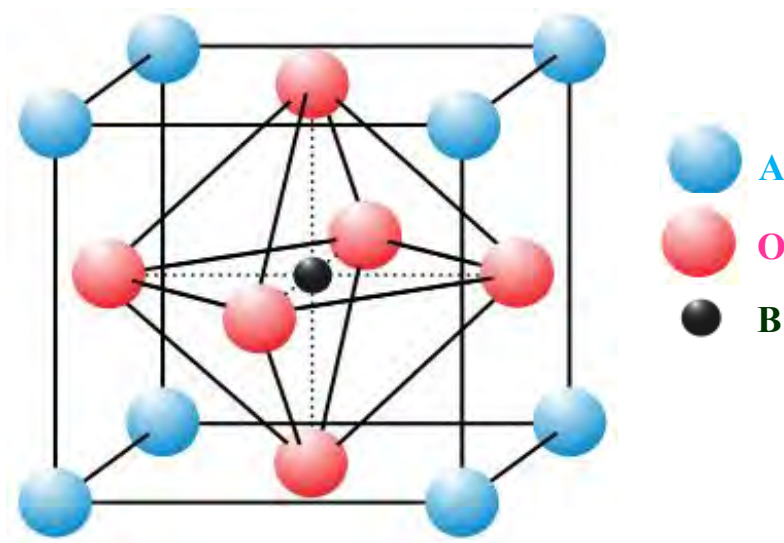


Fig. 2.2 Schematic illustration of ME effect in multiferroic materials [9].

loop and M-H loop at the same temperature (Fig. 2.1) serve as the confirmation of ME effect. In single phase multiferroics the ME effect can be due to the coupling of magnetic and electric orders as observed in some multiferroics. The ME effect in composites is the result of mechanical coupling between ferroelectric (piezoelectric) and ferromagnetic (magnetostrictive) materials. Under applied magnetic field a strain is developed in ferromagnetic (piezomagnetic) material through magnetostriction, which passed to ferroelectric (piezoelectric) material results into stress in it. Thus extra charges are developed across multiferroic composite when magnetic field is applied and vice versa.

## 2.2 Perovskite Structure

Perovskite is a family name of a group of materials and the mineral name of calcium titanate ( $\text{CaTiO}_3$ ) having a structure of the type  $\text{ABO}_3$ . In this structure, the A-site ion, on the



**Fig. 2.3** Perovskite  $\text{ABO}_3$  structure with the A and B cations on the corner and body centre positions, respectively.

corners of the lattice, is usually an alkaline earth or rare earth element. B-site ions, on the center of the lattice, could be 3d, 4d and 5d transitional metal elements. A-site might be occupied by mono-valent, divalent or trivalent metal and B-site might be trivalent, tetravalent or penta-valent metal. A large number of metallic elements are stable in the perovskite structure. Many ferroelectric (including piezoelectric) ceramics such as BT, PT, PZT, PLZT, Lead Magnesium Niobate (PMN), KN etc. have a cubic perovskite type structure (in the paraelectric state) with chemical formula  $ABO_3$  (Fig. 2.4).

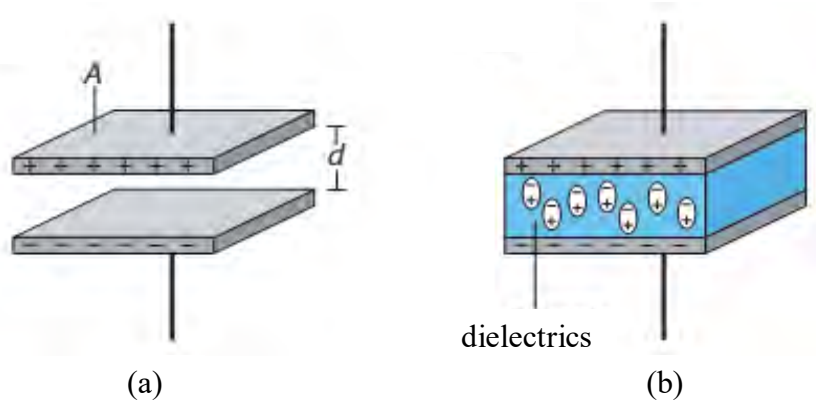
As conventionally drawn, A-site cations occupy the corners of a cube, while B-site cations sit at the body center. Six oxygen atoms per unit cell rest on the faces. The lattice constant of the perovskite structure is usually close to the 4 Å due to rigidity of the oxygen octahedral network and the well-defined oxygen ionic radius of 1.35 Å.

A practical advantage of the perovskite structure is that many different cations can be substituted on both the A and B sites without drastically changing the overall structure. Complete solid solutions are easily formed between many cations, often across the entire range of composition. Even though two cations are compatible in solution, their behaviour can be radically different when apart from each other. Thus, it is possible to manipulate a material's properties such as  $T_C$  or  $\epsilon'$  with only a small substitution of a given cation.

### 2.3 Dielectrics

The word dielectric is derived from the prefix dia, originally from Greek, which means 'through' or 'across', thus the dielectric is referred to as a material that permits the passage of the electric flux but not particles. The dielectric is generally considered a nonconducting or

an insulating material that can be polarized by applying an electric field as shown in Fig. 2.4. When a dielectric is placed in an electric field, electric charges do not flow through the materials as in a conductor, but only slightly shift from their average equilibrium positions causing dielectric polarization. Because of dielectric polarization, positive charges are



**Fig. 2.4** A parallel plate capacitor, where the electrodes are separated by (a) vacuum and (b) a dielectric material.

displaced toward the field and negative charges shift in the opposite direction. This creates an internal electric field which reduces the overall field within the dielectric itself.

An insulator, also called a dielectric, is a material that resists the flow of electric charge. In insulating materials valence electrons are tightly bonded to their atoms. These materials are used in electrical conductors without allowing current through themselves. The study of dielectric properties is concerned with the storage and dissipation of electric and magnetic energy in materials. It is important to explain various phenomenon in electronics, optics and solid state physics.

Dielectrics are broadly divided into two classes: polar dielectrics and non-polar dielectrics. In polar dielectric, a shift has occurred in the atomic structures such that the

positive and negative charges have an asymmetrical alignment producing an electrical dipole. Non-polar dielectric materials lack this inherent dipole in the absence of a polarizing field, however when an external potential is applied, a dipole forms a shift in the electron cloud.

### 2.3.1 Electric polarization

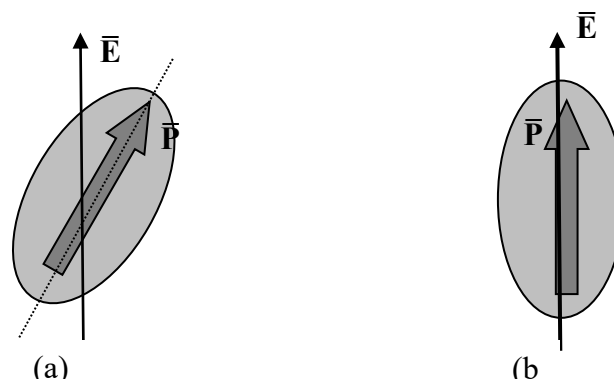
For every dipole, there is a separation between a positive and a negative electric charge. An electric dipole moment ( $\bar{p}$ ) is associated with each dipole as follows:

$$\bar{p} = q \bar{d} \quad (2.2)$$

where,  $q$  is the magnitude of each dipole charge and  $\bar{d}$  is the distance of separation between them. In the presence of an electric field  $\bar{E}$ , which is a vector quantity, a force vector (or torque) will come to bear on an electric dipole to orient it with the applied field; this phenomenon is illustrated in Fig. 2.5 The process of dipole alignment is termed as polarization.

### 2.3.2 Mechanism of polarization

There are several mechanisms of polarization which can contribute to the dielectric response. Each one contributes to dielectric response but at different frequency regimes since they involve different polarizable species. The basic polarization mechanisms are space charge, orientational or dipolar, ionic and electronic (Fig. 2.6). The total polarizability of



**Fig. 2.5** (a) Imposed forces acting on a dipole by an electric field and (b) final dipole alignment

dielectric placed in an alternating field can be written as:  $\alpha_{\text{Tot}} = \alpha_s + \alpha_o + \alpha_i + \alpha_e$ .

**2.3.2.1 Space charge/interfacial polarization (up to  $10^4$  Hz):** It could exist in dielectric material if the density of charge carrier is not homogeneously distributed. This polarization is the slowest process, as it involves the diffusion of ions over several inter-atomic distances. The relaxation time for this process is related to the frequency of successful jumps of ions under the influence of the applied field, a typical value being  $10^2$  Hz. Correspondingly, space charge polarization occurs at lower frequencies ( $10 - 10^4$  Hz). A type of polarization known as Maxwell- Wagner polarization is related to the space charge polarization because this type of polarization is occurred within the frequency range of  $10 - 10^4$  Hz.

**2.3.2.2 Dipolar or orientation polarization (up to  $10^8$  Hz):** It arises when the substance is built up of molecules possessing a permanent electronic dipole moment which may be more or less free to change orientation in an applied electric field. More clearly, according to Debye, this type of polarization is due to the rotation of the molecules of polar dielectrics having a constant dipole moment in the direction of the applied electric field. Orientation polarization is even slower than the ionic polarization. Orientation polarization is both frequency and temperature dependant.

**2.3.2.3 Ionic polarization (up to  $10^{16}$  Hz):** It is due to the displacement of ions over a small distance due to the applied field. Since ions are heavier than electron cloud, the time taken for displacement is large. The frequency with which ions are displaced is of the same order as the lattice vibration frequency ( $\sim 10^{13}$  Hz). It is observed in ionic crystals and occurs up to the infrared region  $10^{16}$  Hz.

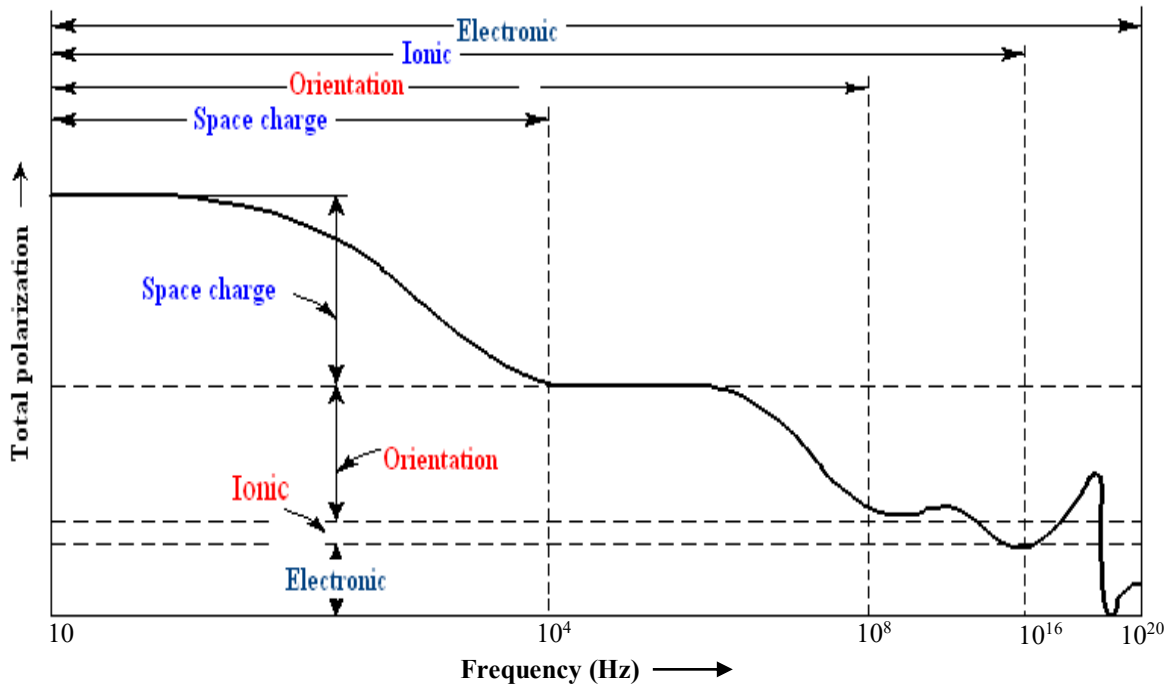


Fig. 2.6 Polarization of a typical dielectric at different frequencies [11].

**2.3.2.4 Electronic polarization (up to  $10^{20}$  Hz):** It exists in all materials (dielectrics as well as all solids) up to frequencies  $10^{20}$  Hz. It is based on the displacement of the negatively charged electron shell against the positively charged core. The displacement occurs due to the equilibrium between restoration and electric forces. Electronic polarization may be understood by assuming an atom as a point nucleus surrounded by spherical electron cloud of uniform charge density. Electronic polarization is extremely rapid. Even when the frequency of applied voltage is very high in optical range, electronic polarization occurs during every cycle of the applied voltage. In general, it is temperature independent.

### 2.3.3 Dielectric Properties

Studies of dielectric properties provide a great deal of information about the suitability of the material for various applications. Dielectric constant ( $\epsilon'$ ), dielectric loss ( $\tan \delta_E$ ) and dielectric break down are important parameters for dielectric materials.



### 2.3.3.1 Dielectric constant

The dielectric constant ( $\epsilon'$ ) of an insulator is given by the relation:

$$\bar{D} = \epsilon' \bar{E} = \epsilon_0 \epsilon' E_0 \quad (2.3)$$

where,  $\bar{D}$  represents the electric displacement,  $\bar{E}$  the electric field in the dielectric,  $\epsilon'$  the dielectric constant and  $\epsilon_0$  permittivity in vacuum. The electric displacement describes the extent to which the electric field has been altered by the presence of the dielectric material. The  $\epsilon'$  is an intrinsic property of a material and a measure of the ability of the material to store electric charge relative to vacuum. It is measured indirectly from the capacitance of a capacitor in which the material is used as electrode separator or dielectric. From Eq. (2.3) and the capacitive cell that describes in Fig. 2.7 the  $\epsilon'$ , total charge Q (Coulombs) and capacitance C (Farads) can be developed as follows:

$$\epsilon' = \frac{\bar{D}}{\epsilon_0 E_0} = \frac{Q/A}{\epsilon_0 V/d} \quad (2.4)$$

Therefore, 
$$Q = \epsilon_0 \epsilon' \frac{A}{d} V = CV \quad (2.5)$$

where, 
$$C = \epsilon_0 \epsilon' \frac{A}{d} \quad (2.6)$$

Capacitance in vacuum is given by, 
$$C_0 = \epsilon_0 \frac{A}{d} \quad (2.7)$$

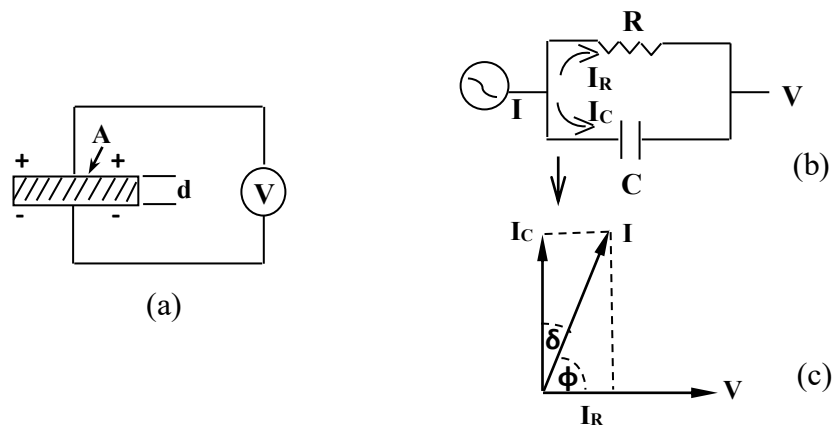
and hence, 
$$\epsilon' = \frac{C}{C_0} \quad (2.8)$$

where, A represents the area of the capacitive cell, d its thickness (or gap between the electrodes),  $C_0$  and C are the respective capacitances of the capacitor with air and material and V is the voltage across the cell. Thus,  $\epsilon'$  represents the ratio of the permittivity or charge storage capacity relative to air or vacuum as dielectric. A real capacitor can be represented with a

capacitor and a resistor. It is clear from Eq. (2.8) that for a given size capacitor and applied voltage, the higher the  $\epsilon'$  the higher the capacitance of the capacitor. This is the only variable left with the material scientist to increase the capacitance per unit volume value of capacitor for modern electronics applications.

### 2.3.3.2 Dielectric loss

Friction is a macroscopic concept and its explanation in terms of models conceived at a microscopic level has presented difficulties in many branches of physics. Dielectric loss is a special type of friction and the classical and quantum statistical mechanical theories of dielectric loss present the familiar difficulties of principle encountered in a theory of dissipation. Every type of dissipation (dielectric loss) is connected with motions of charge carrier. The effect of their movements in an electric field is called polarization. The total polarization is the sum of various contributions, e.g. electronic polarization due to the relative displacement of electrons and nuclei, dipolar polarization due to orientation of dipoles, ionic polarization due to the relative displacement of ions and interfacial or Maxwell-Wagner



**Fig. 2.7** Equivalent circuit diagrams: **a)** capacitive cell, **b)** charging loss current and **c)** loss tangent.

polarization when there are boundaries between the components of a heterogeneous system as mentioned above. The occurrence of dielectric loss can generally be understood as follows: at very low frequencies the polarization easily follows the alternating field, thus its contribution to the  $\epsilon'$  is maximum and no loss occurs. At very high frequencies the field alternates too fast for polarization to arise and there is no contribution to the value of  $\epsilon'$  and no energy is lost in the medium. Somewhere between these two extremes the polarization begins to lag behind the field and energy is dissipated. An ideal dielectric would allow no flow of electronic charge, only a displacement of charge via polarization. If a plate of such ideal material was placed between the capacitive cell shown in Fig. 2.9 and a dc voltage was applied, the current through the circuit would decay exponentially to zero with time. But this would not be case if an alternating (sine wave) electric field was applied. In this case Eq. (2.5) may be written as:

$$Q = CVe^{i\omega t} \quad (2.9)$$

Therefore, 
$$I = \frac{dQ}{dt} = i\omega\omega_0 CV = i\omega\omega_0\epsilon_0\epsilon'V \quad (2.10)$$

Here,  $I$  represents the current flow on discharge of the capacitor in time  $t$ . For real dielectric material, the current  $I$  has two vector components, real  $I_R$  and imaginary  $I_C$ . The condition of loss (not so good) is illustrated in Fig. 2.9 (b) which is an equivalent circuit analogous of a resistance in parallel with the capacitor. The current  $I_C$  represents a (watt less) capacitive current proportional to the charge stored in the capacitor. It is frequency dependent and leads the voltage by  $90^\circ$ . On the other hand, the current  $I_R$  is ac conduction current in phase with the voltage  $V$ , which represents the energy loss or power dissipated in the dielectric. The resultant angle between the current and the voltage is  $\phi$  somewhat less than  $90^\circ$ . The current in real capacitor lags slightly behind what it would be in an ideal capacitor. The angle of lag is defined

as  $\delta$  and the amount of lag becomes  $\tan \delta_E$  or loss tangent. Eq. (2.10) can be written for real and imaginary part,

$$I = I_R + I_C \quad (2.11)$$

$$= \omega C_0 \varepsilon_0 \varepsilon' V + i \omega \omega_0 \varepsilon_0 \varepsilon'' V \quad (2.12)$$

By definition, 
$$\tan \delta_E = \left| \frac{I_C}{I_R} \right| = \frac{\varepsilon''}{\varepsilon'} \quad (2.13)$$

Dielectric loss often attributed to ion migration, ion vibration and deformation and electric polarization. Ion migration is particularly important and strongly affected by temperature and frequency. The losses due to ion migration increase at low frequency and with the increase in temperature.

### 2.3.4 Dependence of dielectric properties on various factors

$\varepsilon'$  is the property of a dielectric medium that determines the force of the electric charges that exerts on the dielectric. The value of  $\varepsilon'$  depends on the several external factors, such as the frequency of the voltage applied to the dielectric, temperature, particle size etc.

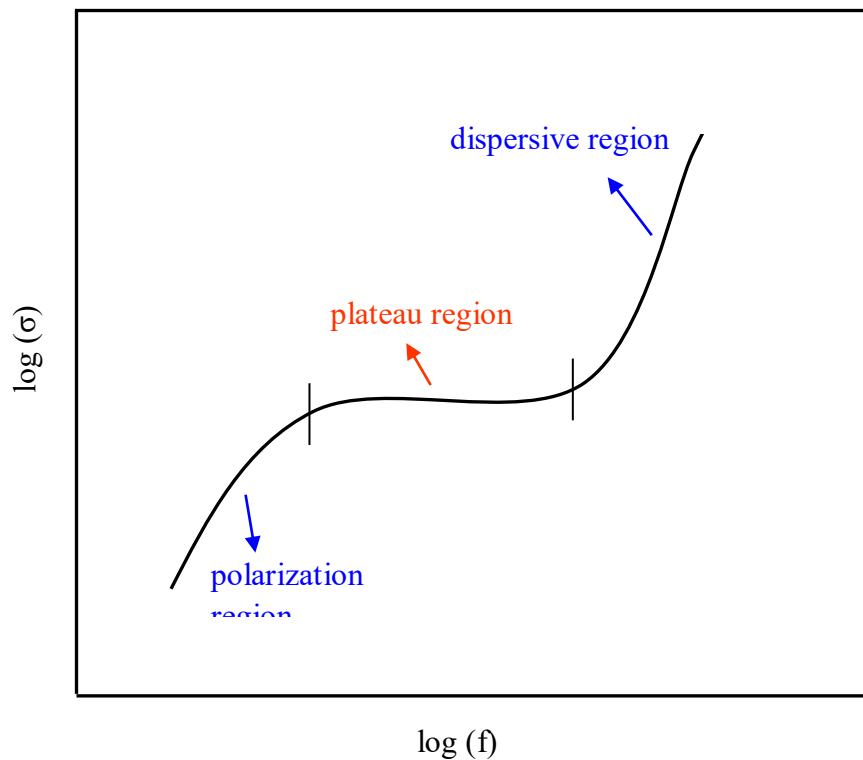
#### 2.3.4.1 Dependence of dielectric constant on frequency

The time required for electronic or ionic polarization to set in, is very small as compared with the time of voltage sign change with the half period of alternating voltage, even of the highest frequencies which find practical use in electrical and radio engineering. For this reason, the polarization of deformational mechanism of polarization, completely settles itself during a very short period of time as compared with voltage half period. The value of  $\varepsilon'$  of non-polar dielectrics does not depend on frequency when it changes within very broad limits.

The value of  $\varepsilon'$  depends on frequency only in the case of polar dielectrics. When the frequency of alternative voltage increases the value of  $\varepsilon'$  of a polar dielectric at first remains invariable but above a certain critical frequency ' $f_o$ ' (when polarization fails to settle itself completely during one half periods)  $\varepsilon'$  begins to drop approaching. At very high frequencies,  $\varepsilon'$  behaves like the typical value of non-polar dielectrics.

### 2.3.5 Jonscher's power law

Electrical conductivity of solid materials as a function of frequency can generally be described as frequency independent, dc conductivity ( $\sigma_{dc}$ ) and a strongly frequency dependent components.



**Fig. 2.8** Schematic representation of  $\log(\sigma)$  vs  $\log(f)$ .

A typical frequency dependence of conductivity spectrum shown in the Fig. 2.12 exhibits three distinguish regions; (a) low frequency dispersion (b) an intermediate frequency plateau and (c) an extended dispersion at high frequency. The variation of conductivity in the low frequency region is attributed to the polarization effects at the electrode and materials interface. As the frequency reduces, more and more, charge accumulation occurs at the electrode and material interface and hence, drop in conductivity. In the intermediate frequency plateau region, conductivity is almost found to be frequency independent and is equal to  $\sigma_{dc}$ . In the high frequency region, the conductivity increases with the frequency and is equal to  $\sigma_{AC}$ . The frequency dependence of conductivity or so-called universal dynamic response (UDR) of ionic conductivity is related by a simple expression given by Jonscher's power law [16],

$$\sigma(\omega) = \sigma(0) + A\omega^s \quad (2.19)$$

where,  $\sigma(\omega)$  is the ac conductivity,  $\sigma(0)$  is the limiting zero frequency conductivity  $\sigma_{dc}$ , A is a pre-exponential constant,  $\omega = 2\pi f$  is the angular frequency and 's' is the power law exponent, where  $0 < 's' < 1$ . Both A and 's' are temperature and material dependent [16].

## 2.4 Magnetization

Magnetization is the vector field that expresses the density of permanent or induced magnetic dipole moments in a magnetic material. The origin of the magnetic moments responsible for magnetization can be either microscopic electric currents resulting from the motion of electrons in atoms or the spin of the electrons or the nuclei. Net magnetization results from the response of a material to an external magnetic field, together with any unbalanced magnetic dipole moments that may be inherent in the material itself; for example,

in ferromagnets. Magnetization is not always homogeneous within a body, but rather varies between different points. Magnetization also describes how a material responds to an applied magnetic field as well as the way the material changes the magnetic field and can be used to calculate the forces that result from those interactions. It can be compared to electric polarization, which is the measure of the corresponding response of a material to an electric field in electrostatics. Physicists and engineers define magnetization as the quantity of magnetic moment per unit volume. It is represented by a vector  $\bar{M}$ .

Mathematically, magnetization can be defined according to the following equation:

$$\bar{M} = \left(\frac{N}{V}\right) \bar{m} = n\bar{m} \quad (2.20)$$

Here,  $\bar{M}$  represents magnetization;  $\bar{m}$  is the vector that defines the magnetic moment;  $V$  represents volume and  $N$  is the number of magnetic moments in the sample. The quantity  $N/V$  is usually written as  $n$ , the number density of magnetic moments. The  $\bar{M}$  is measured in amperes per meter (A/m) in SI units.

### Relations between $\bar{B}$ , $\bar{H}$ and $\bar{M}$

The magnetization defines the auxiliary magnetic field  $\bar{H}$  as,

$$\bar{B} = \mu_0 (\bar{H} + \bar{M}) \text{ (SI units)} \quad (2.21)$$

which is convenient for various calculations. The vacuum permeability ( $\mu_0$ ) is, by definition,  $4\pi \times 10^{-7} \text{ V}\cdot\text{s}/(\text{A}\cdot\text{m})$

#### 2.4.1 Ferro-, antiferro- and ferri-magnetic properties

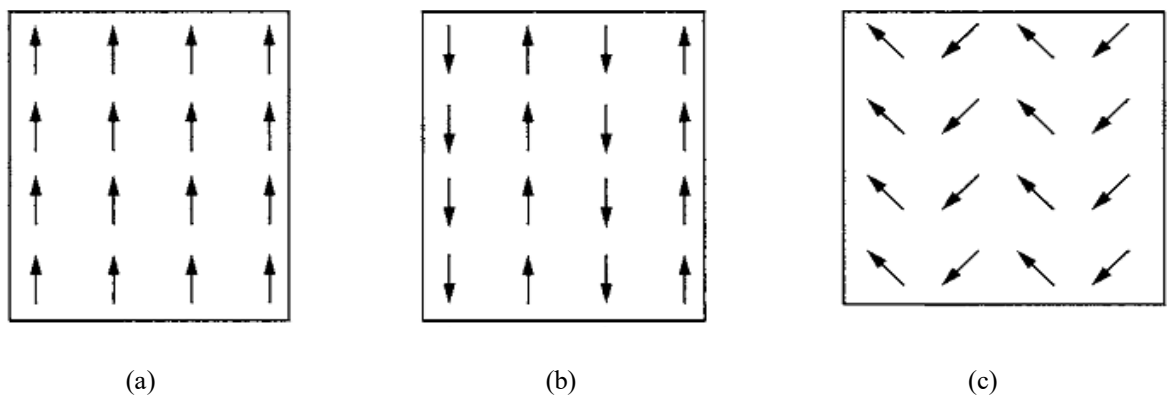
The phenomenon of magnetism has been known to mankind for many thousands of years. Magnetic materials have magnetic moment analogous to electric dipole moment. The magnetic moment of an atom/ ion has three principal sources:

(1) the spin of electrons

- (2) electron orbital angular momentum about the nucleus and
- (3) a change in the orbital moment induced by an applied magnetic field.

The first two effects give paramagnetic contributions to the magnetization and the third gives a diamagnetic contribution.

In a crystal, the overall magnetic property depends on two factors: i) the magnetic response associated with each atom/ion and ii) the interactions between these magnetic moments. In the case, where there are no unpaired electrons in atoms/ions, there will be no net magnetic moments associated with them; these material will show diamagnetic behaviour. When there are unpaired electrons, every atom/ion has a net magnetic moment. Depending on the interactions between the magnetic dipoles or order of magnetic moments, the material may show (i) paramagnetism (ii) ferromagnetism (iii) antiferromagnetism and (iv) ferrimagnetism. In a paramagnetic material, alignment of adjacent moments is not observed due to thermal fluctuation. Ferromagnetism consists of parallel aligned adjacent moments (Fig. 2.9 (a)). Antiferromagnetic order consists of antiparallel aligned equal moments (Fig. 2.9 (b)) resulting a zero net magnetization. And ferrimagnetic order consists of antiparallel unequal moments (Fig. 2.9 (c)), resulting in a non-zero net magnetization.



**Fig. 2.9** Schematic illustration of magnetic dipole ordering in (a) ferromagnetic (b) antiferromagnetic and (c) ferrimagnetic structure.



Ferromagnetism is a very strong magnetic response compared with paramagnetic and diamagnetic behaviors. It is characterized by a transition temperature (Curie temperature,  $T_C$ ). Above this temperature, the material is paramagnetic. Below this temperature, it is ferromagnetic. The magnetic susceptibility,  $\chi = \frac{\bar{M}}{H}$ , which defines the degree of magnetization of a material in response to a magnetic field, is a good indication of their magnetic properties. If  $\chi$  is positive, the material is paramagnetic and the magnetic field is strengthened by the presence of the material. If  $\chi$  is negative, the material is diamagnetic and the magnetic field is weakened in the presence of the material. The magnetic susceptibility of a ferromagnetic substance is not linear.

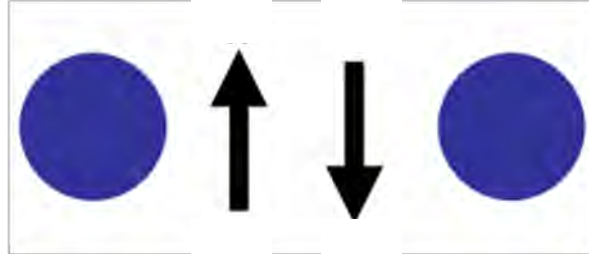
#### 2.4.2 Magnetic exchange interaction

Magnetism can be divided into two groups, group A and group B. In group A there is no interaction between the individual moments and each moment acts independently of the others. Diamagnets and paramagnets belong to this group.

Group B consists of the magnetic materials in which magnetism occurs because the magnetic moments couple to one another and form magnetically ordered states. The coupling, which is quantum mechanical in nature, is known as the exchange interaction and is rooted in the overlap of electrons in conjunction with Pauli's exclusion principle. Whether it is a ferromagnet, antiferromagnet or ferrimagnet the exchange interaction between the neighboring magnetic ions will force the individual moments into parallel (ferromagnetic) or antiparallel (antiferromagnetic) alignment with their neighbors. The three types of exchange interaction which are currently believed to exist are: a) direct exchange, b) superexchange and c) Dzyaloshinskii-Moriya (DM) interaction.

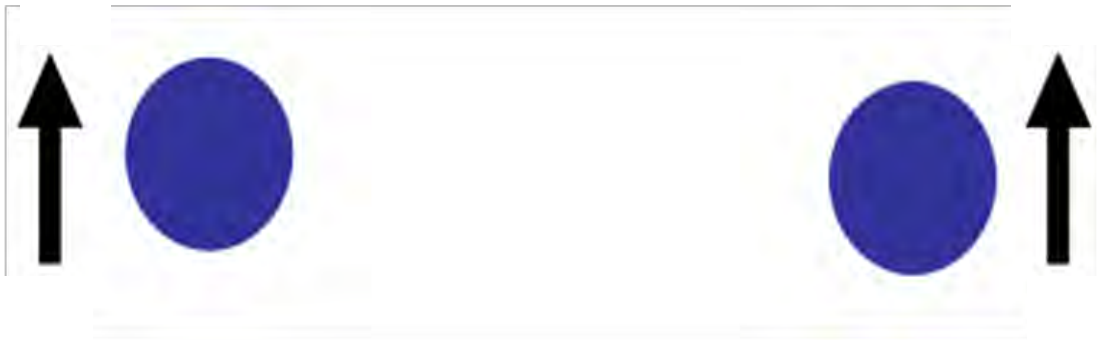
### 2.4.2.1 Direct exchange interaction

When the atoms are very close together the Coulomb interaction is minimal then the electrons spend most of their time in between the nuclei. Since the electrons are then required



**Fig. 2.10** Antiparallel alignment for small interatomic distances.

to be at the same place in space at the same time, Pauli's exclusion principle requires that they possess opposite spins. According to Bethe and Slater, the electrons spend most of their time in between neighboring atoms when the interatomic distance is small. This gives rise to antiparallel alignment and therefore negative exchange (antiferromagnetic), Fig. 2.14.



**Fig. 2.11** Parallel alignment for large interatomic distances.

If the atoms are far apart, the electrons spend their time away from each other in order to minimize the electron-electron repulsion. This gives rise to parallel alignment or positive exchange (ferromagnetism) as shown in Fig. 2.11.

### 2.4.2.2 Superexchange interaction

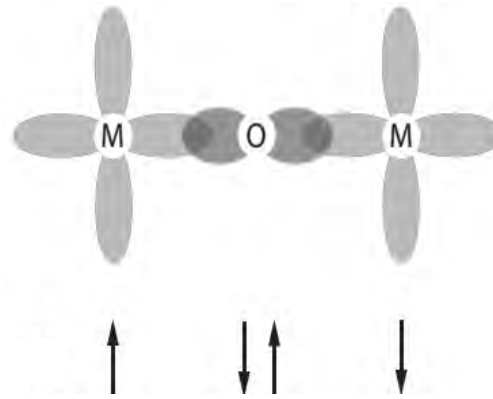


Fig. 2.12 Superexchange interaction.

Superexchange interaction between two magnetic atoms is occurred via some intermediate process (e.g. via oxygen atom). Superexchange is a result of the electrons having come from the same donor atom and being coupled with the receiving ions' spins. It favors antiferromagnetic interaction. If the two next-to-nearest neighbor positive ions are connected at  $90^\circ$  to the bridging non-magnetic anion (oxygen atom), the interaction can be a ferromagnetic interaction. Fig. 2.12 shows superexchange interaction between two magnetic atoms.

### 2.4.2.3 Dzyaloshinskii-Moriya interaction

Antisymmetric exchange interaction between two neighboring magnetic spins is occurred via spin-orbit coupling rather than oxygen ion (Fig. 2.13). It is called Dzyaloshinskii-Moriya (DM) interaction. It favours non-collinear spin ordering, resulting in weak ferromagnetic. The

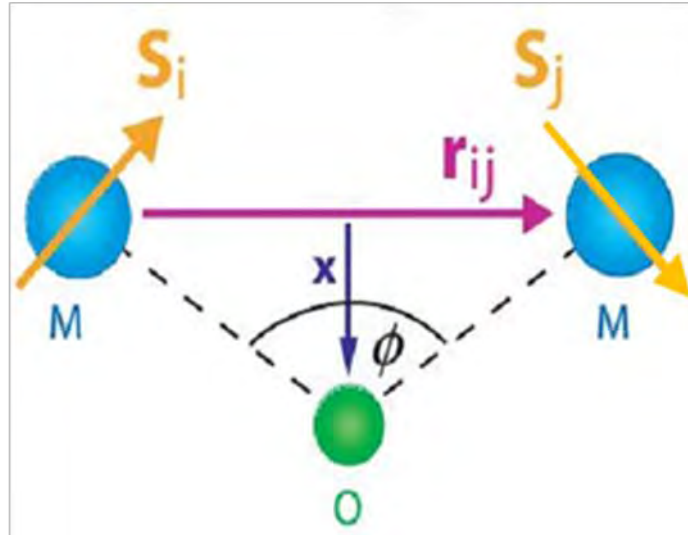


Fig. 2.13 Schematic diagram of Dzyaloshinskii-Moriya (DM) interaction.

spin-orbit coupling can be written as:  $\hat{H}_{DM} = \bar{D}_{ij} \cdot [\bar{S}_i \times \bar{S}_j]$ , where,  $\bar{D}_{ij}$  is so called Dzyaloshinskii-Moriya vector. The antisymmetric exchange is of importance for the understanding of magnetism induced electric polarization in a recently discovered class of multiferroics (e.g. BiFeO<sub>3</sub>). Here, small shifts of the legend ions can be induced by magnetic ordering because the system tends to enhance the magnetic interaction energy on the cost of lattice energy.

### 2.4.3 Theories of permeability

Permeability ( $\mu$ ) is defined as the proportionality constant between the magnetic field induction  $\bar{B}$  and applied field intensity  $\bar{H}$ :

$$\bar{B} = \mu \bar{H} \quad (2.22)$$

If the applied field is very low, approaching zero, the ratio is called the initial permeability ( $\mu_i$ ) and is given by,

$$\mu_i = \frac{\Delta B}{\Delta H} \quad (2.23)$$

This simple definition needs further sophistications. A magnetic material subjected to an AC magnetic field can be written as

$$H = H_0 e^{i\omega t} \quad (2.24)$$

It is observed that the magnetic flux density  $\bar{B}$  lag behind  $\bar{H}$ . This is caused due to the presence of various losses and is thus expressed as

$$B = B_0 e^{i(\omega t - \delta)} \quad (2.25)$$

Here  $\delta$  is the phase angle that marks the delay of  $\bar{B}$  with respect to  $\bar{H}$ . The permeability is then given by



$$\mu = \frac{B}{H} \quad (2.26)$$

where 
$$\mu' = \frac{B_0}{H_0} \cos \delta \quad (2.27)$$

and 
$$\mu'' = \frac{B_0}{H_0} \sin \delta \quad (2.28)$$

The real part of complex permeability ( $\mu'$ ), as expressed in Eq. (2.27) represents the component of  $\bar{B}$  which is in phase with  $\bar{H}$ , so it corresponds to the normal permeability. If there are no losses, it should have  $\mu = \mu'$ . The imaginary part ( $\mu''$ ) corresponds to that of  $B$ , which is delayed by phase angle  $90^\circ$  from  $\bar{H}$ . The presence of such a component requires a supply of energy to maintain the alternating magnetization, regardless of the origin of delay. The ratio of  $\mu''$  to  $\mu'$ , as is evident from Eq. (2.27) and (2.28) gives,

$$\frac{\mu''}{\mu'} = \frac{\frac{B_0}{H_0} \sin \delta}{\frac{B_0}{H_0} \cos \delta} = \tan \delta_M \quad (2.29)$$

This  $\tan \delta_M$  is called magnetic loss factor.

The quality factor is defined as the reciprocal of this loss factor, i.e.

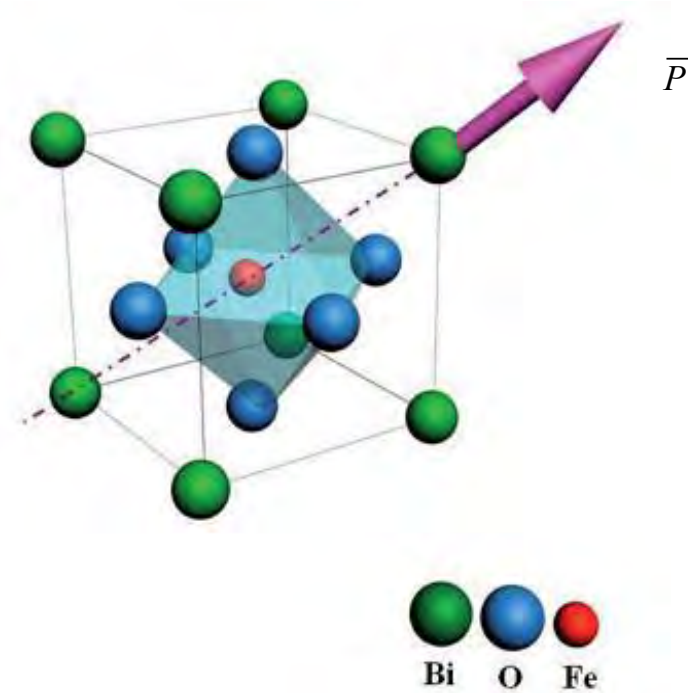
$$\text{Quality factor, } Q = \frac{1}{\tan \delta_M} \quad (2.30)$$

And the relative quality factor,  $RQF = \frac{\mu'}{\tan\delta_M}$  (2.31)

The curves that show the variation of both  $\mu'$  and  $\mu''$  with frequency are called the magnetic spectrum or permeability spectrum of the material. The variation of permeability with frequency is referred to as dispersion. The measurement of complex permeability gives us valuable information about the nature of domain wall and their movements. In dynamic measurements the eddy current loss is very important. This occurs due to the irreversible domain wall movements. The permeability of a ferromagnetic substance is the combined effect of the wall permeability and rotational permeability mechanisms.

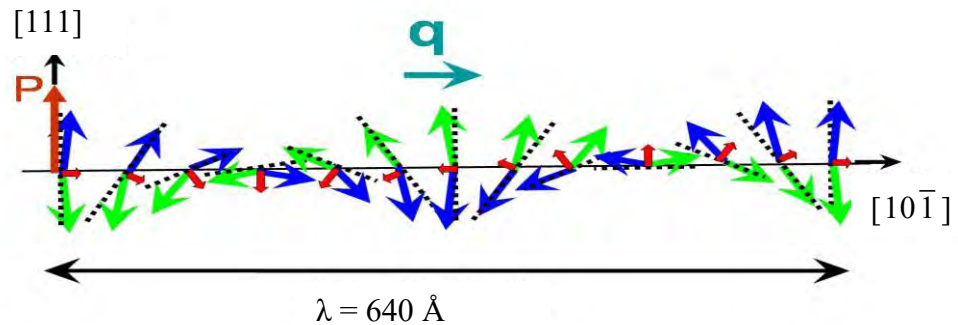
## 2.5 Multiferroic material BiFeO<sub>3</sub>

Multiferroic materials having ABO<sub>3</sub> structure are rare in nature because the criteria for being simultaneously ferroelectric and ferro/antiferromagnets are mutually exclusive. Ferroelectricity prefers the d<sup>0</sup> (empty d-shell) electronic configuration for the B-cation and ferromagnetism prefers partially filled 'd' of B cation. Perovskite structured material BFO don't have the criteria but it exhibits multiferroic properties at and above room temperature. The "6s" lone pair electrons of Bi<sup>3+</sup> are believed to be responsible for ferroelectricity while partially filled 'd' orbital's of Fe<sup>3+</sup> in BFO leads to magnetic ordering [17]. BFO exhibits an antiferromagnetic (weak ferromagnetic) behavior with a relatively high Néel temperature (T<sub>N</sub> = 370 °C) and ferroelectric behavior with a high Curie temperature (T<sub>C</sub> = 810 °C) and possesses a rhombohedrally distorted perovskite structure (Fig. 2.14). Magnetic ordering of BFO is G- type antiferromagnetic [18] that is; each Fe<sup>3+</sup> spin is



**Fig. 2.14** Rhombohedrally distorted perovskite structure of BFO [18] with the polarization vector  $\bar{P}$ .

surrounded by six antiparallel spins on the nearest Fe neighbors. Direction of polarization is shown in Fig. 2.14. The weak ferromagnetic property exhibits by the BFO is caused by residual moment that make the canted  $\text{Fe}^{3+}$  spin structure. The antiferromagnetic spin but is



**Fig. 2.15** Schematics of the 640 Å antiferromagnetic cycloid [19].

manifested as an incommensurate cycloid structure with a wavelength of  $\sim 640$  Å [19] along the direction as can be seen in Fig. 2.15.

**References**

- [1] Schmid, H., “Multi-ferroic magnetoelectric”, *Ferroelectrics*, Vol. 162, pp. 317- 338, 1994.
- [2] Wang, J., Neaton, J. B., Zheng, H., Nagarajan, V., Ogale, S. B., Liu, B., Viehland, D., Vaithyanathan, V., Schlom, D. G., Waghmare, U. V., Spaldin, N. A., Rabe, K. M., Wuttig, M. and Ramesh, R., “Epitaxial BiFeO<sub>3</sub> multiferroic thin film heterostructures”, *Science*, Vol. 299, pp. 1719-1722, 2003.
- [3] Kimura, K., Goto, T., Shintani, H., Ishizaka, K., Arima, T. and Tokura, Y., “Magnetic control of ferroelectric polarization” *Nature*, Vol. 426, pp. 55-58, 2003.
- [4] Hur, N., Park, S., Sharma, P. A., Ahn, J. S., Guha, S. and Cheong, S. W., “Electric polarization reversal and memory in a multiferroic material induced by magnetic fields”, *Nature*, Vol. 429, pp. 392–395, 2004.
- [5] Spaldin, N. A. and Fiebig, M., “The Renaissance of magnetoelectric multiferroics”, *Science*, Vol. 309, pp. 391-392, 2005.
- [6] Dzyaloshinskii, I. E., “On the magneto-electrical effects in antiferromagnets”, *Zh. Eksp. Teor. Fiz.*, Vol. 37, pp. 881–882, 1959 [*Sov. Phys. JETP*, Vol. 10, pp. 628–629, 1959].
- [7] Astrov, D. N., “The magnetoelectric effect in antiferromagnetics”, *Zh. Eksp. Teor. Fiz.*, Vol. 38, pp. 984–985, 1960 [*Sov. Phys. JETP*, Vol. 11, pp. 708–709, 1960].
- [8] Smolenski, G. A. and Chupis, I. E., “Ferro electromagnets”, *Usp. Fiz. Nauk.*, Vol. 137, pp. 415–448, 1982, [*Sov. Phys. Usp.*, Vol. 25, pp. 475-493, 1982].
- [9] Tokura, Y. and Seki, S., “Multiferroics with spiral spin orders”, *Adv. Mater.*, Vol. 22, pp. 1554-1565, 2010.
- [10] Goldschmidt, V. M., “The laws of crystal chemistry”, *Naturwissenschaften*, Vol. 14, pp. 477-485, 1926.
- [11] Pelaiz-Barranco, A. and Guerra, J. D. S., “Dielectric relaxation phenomenon in ferroelectric perovskite related structures”, *Edited by Indrani Coondoor*, Published by In Tech, Rijeka, Croatia, 2010.
- [12] Kingery, W. D., Bowen, H. K. and Uhlman, D. R., *Introduction to Ceramics*, Second ed., New York, 1976.
- [13] Davidson, D. W. and Cole, R. H. , “Dielectric relaxation in glycerine”, *J. Chem. Phys.*, Vol. 18, pp. 1417-1417, 1950.
- [14] Havriliak, S. and Negami, S., “A complex plane analysis of  $\alpha$ -dispersions in some polymer systems”, *J. Polymer Sci. Pt. C.*, Vol. 14, pp. 99-117, 1966.



- [15] Fuoss, R. M. and Kirkwood, J. G., “Electrical properties of solids. VIII. dipole moments in polyvinyl chloride-diphenyl systems”, *J. Amer. Chem. Soc.*, Vol. 63, pp. 385-394, 1941.
- [16] Joncher, A. K., “The universal dielectric response”, *Nature*, Vol. 267, pp. 673-679, 1977.
- [17] Hill, N., “Why are there so few magnetic ferroelectrics?”, *J. Phys. Chem. B*, Vol. 104, pp. 6694-6709, 2000.
- [18] Wodecka-Du's, B. and Czekaj, D., “Synthesis of 0.7BiFeO<sub>3</sub>–0.3BaTiO<sub>3</sub> ceramics: thermal, structural and ac impedance studies”, *Archives of metallurgy and materials*, Vol. 56, pp. 1127-1136, 2011.
- [19] Lebeugle, D., Colson, D., Forget, A., Viret, M., Bataille, A. M. and Gukasov, A., “Electric-field induced spin flop in BiFeO<sub>3</sub> single crystals at room temperature”, *Phys. Rev. Lett.*, Vol. 100, pp. 227602-227603, 2008.

## CHAPTER 3

### SAMPLE PREPARATION AND EXPERIMENTAL TECHNIQUES

#### 3.1 Introduction

The preparation of polycrystalline ceramics with optimum desired properties is still a complex and difficult task and control of the chemical composition, homogeneity and microstructure are very crucial. As most of the properties needed for ceramics applications are not intrinsic but extrinsic, preparation of samples has to encounter added complexity. Several methods that are followed to prepare ceramic materials:

- 1) Solid state reaction
- 2) Sol-gel synthesis
- 3) Co-precipitation technique
- 4) Auto-combustion synthesis

Nowadays, the majority of ceramic powders are made by the conventional ceramic process or standard solid state reaction technique. The standard solid state reaction technique has been used in this research work. The technique is described below.

#### 3.1.1 Standard solid state reaction technique

A solid state reaction is a direct reaction between starting reagents (usually powders) at high temperature. High temperature provides the necessary energy for the reaction to occur. Solid state reaction is usually slow because during the reaction, a large amount of bonds break and the ions migrate through a solid unlike gas phase and solution reactions. The limiting factor in solid state reaction is usually diffusion. So the rate controlling step in a solid state reaction is the diffusion of the cations through the product layer. Solid state reaction occurs much more quickly with increasing temperature and reaction does not

normally occur until the reaction temperature reaches at least 2/3 of the melting point of one of the reactants.

In solid state reaction method, raw materials are weighed out according to the stoichiometry of the compound with due consideration for impurity and moisture contents. Raw materials are mechanically mixed and then grinding operations are performed to control the particle size and to mixture homogeneously. For this purpose milling operation is performed which can reduce the particle size to 1-10  $\mu\text{m}$  range [1]. An attempt to reduce the size of the particles further may affect the homogeneity and purity of the material. Distilled water or alcohol is used as wetting medium as it is available with adequate purity at low cost and is non-inflammable. Next step is to occur the solid state reaction between the constituents of starting materials at suitable temperature. This process is called firing or calcinations. During calcinations, control over stoichiometry is essential and hence the volatile constituents have to be compensated. Calcination causes the constituents to interact by inter diffusion of the ions and resulting in a homogeneous body. Hence it is considered that calcinations are the part of the mixing process. Calcination also controls the shrinkage during sintering. After calcinations the powder is compacted to give desired shape, known as green body and then the green body is densified through sintering. A general discussion on calcinations and sintering is given below.

### 3.1.2 Synthesis of samples for the present research

Various  $\text{Bi}_{0.9-x}\text{Ca}_{0.1}\text{Y}_x\text{Fe}_{0.9}\text{Zr}_{0.1}\text{O}_3$  (where,  $x=0.00, 0.05, 0.10, 0.15, 0.20$ ) were prepared by standard solid state reaction method. Raw materials of high purity  $\text{Bi}_2\text{O}_3$  (99.9%),  $\text{CaCO}_3$  (99.9%),  $\text{Y}_2\text{O}_3$  (99.9%),  $\text{Fe}_2\text{O}_3$  (99.9%),  $\text{ZrO}_2$  (99.9%) were mixed thoroughly in both dry and acetone media using an agate mortar and pestle.

### 3.1.3 Calcination schedule

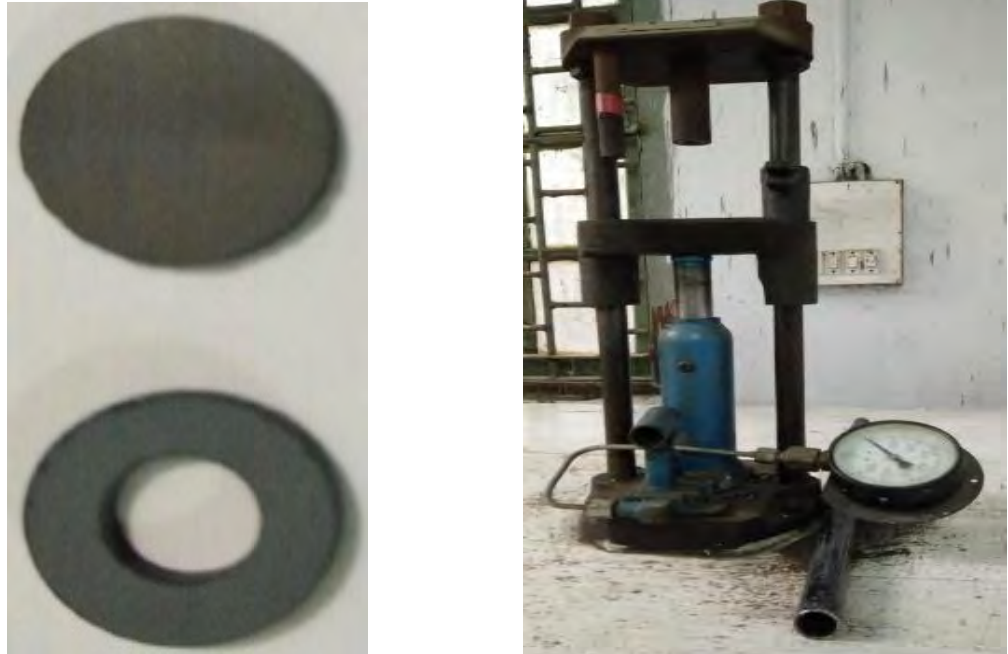
Calcination is a chemical reaction process during which either the partial or complete phase of the compound is formed. It also helps in removing the unwanted gases and products during the decomposition of the constituent compounds. Calcination also helps in homogenizing the materials and reducing the shrinkage during the subsequent sintering process of the finally shaped samples.

Synthesis of the phase of a compound takes place by solid phase reaction, which involves the chemical reaction through atomic diffusion among grains at temperature below the melting points of the raw materials [2]. Usually, the calcination temperature is chosen high enough to cause reaction, but low enough to facilitate subsequent grinding. In the materials, having volatile constituents, the calcination temperature must be kept low enough to avoid loss of the volatile parts.

The grinded powder were calcined in air at 750°C for 1 h. The calcined powders will then be ground in to fine powders. From the fine powders, toroid- and disk-shaped samples will be prepared and sintered at various temperatures (below the melting point of the materials).

### 3.1.4 Preparation of green body

Calcined powders are ball milled again to give suitable shaping to the powder. Then uniaxial pressing is used to make compact samples with small size of the calcined powder. It is carried out in a die having movable top. A cavity is formed at the bottom in lower portion. This cavity is filled with free flowing granulated powder and it is stuck with the top to die. With the help of the top-punch, pressure of 45 MPa is applied using a Hydraulic press. To make a pellet of 0.9 g and toroidal shaped ring of 0.6 g powders are taken from the calcined powders.



**Fig. 3.1** (a) Disks and toroid shaped samples and (b) Uniaxial press machine.

### 3.1.5 Sintering

Sintering is the process in which the green compacts are consolidated into strong and dense polycrystalline aggregates. During sintering at an appreciable temperature, the atomic motion is more violent and the area between grains in contact inverses due to the thermal expansion of the grains and finally only one interface between two grains remains. This corresponds to a state with much lower surface energy. In this state, the atoms on the grain surfaces are affected by neighboring atoms in all directions, which results in densified ceramic [2].

Sintering of crystalline solids is dealt by Coble and Burke [5] who described an empirical relationship regarding rate of grain growth is given below:

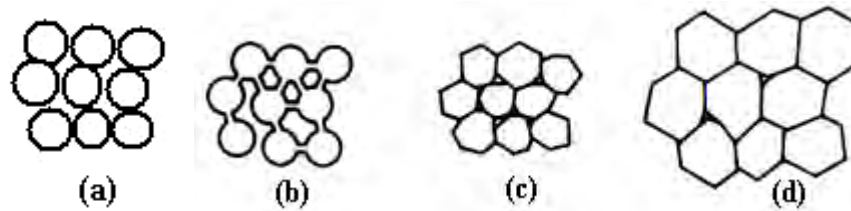
$$D = kT^n \quad (3.1)$$

where,  $D$  is the mean grain diameter,  $n$  is about  $1/3$ ,  $T$  is sintering time and  $k$  is a temperature dependent parameter. Sintering is divided into three stages, Fig. 3.2.

Stage 1. Contact area between particles increases,

Stage 2. Porosity changes from open to close porosity,

Stage 3. Pore volume decreases; grains grow.



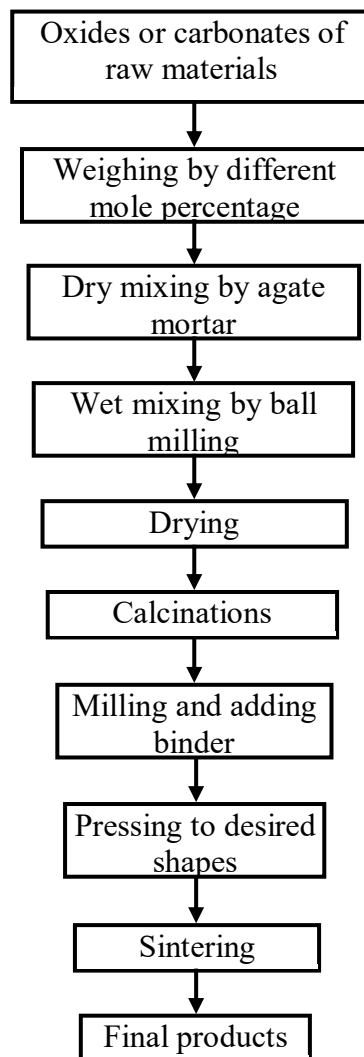
**Fig. 3.2** Schematic representation of sintering stages: **(a)** green body, **(b)** initial stage, **(c)** intermediate stage and **(d)** final stage.

At the beginning of the sintering process, but rather at high temperature, the lattice distortion and internal strain are reduced by atomic diffusion and this is frequently called as the recovery process. When the temperature increases further, a recrystallization process takes place through atomic diffusion. During recrystallization, new crystal nuclei form and grow at grain boundaries and in other regions inside the grain with higher free energies. Meanwhile some grains grow by swallowing up other smaller grains. In the recrystallization stage grain growth is usually realized through the motion of grain boundaries. In general, higher the sintering temperature, larger the grains would grow, as the grain growth is caused by atomic diffusion, which increases with the increase in sintering temperature. However, the density of ceramic is affected by the sintering temperature and time in a more complex fashion. If the sintering temperature is too high or the sintering time is too long, the density of the alkaline based ceramics are reduced owing to BaO evaporation at high temperature. Since, the grain growth is caused by atomic diffusion; it follows that a higher sintering temperature and a larger hold time would result in larger grains.

The pellets and rings were placed in boat and inserted into the furnace for sintering. Sintering was done at 850°, 870°, 890°, 910° and 930°C for 4 hours. The temperature rate was 10°C/min for heating and 5°C/min for cooling. The pellets and rings were then polished to have a smooth faces and both were ready to measurements.

### 3.1.6 The stages in preparation of sample

The flow chart for the preparation of samples by solid-state reaction technique is described in Fig. 3.3.



**Fig. 3.3** Flow chart of the stages in preparation of sample by solid state reaction technique.

### 3.2 Characterization Techniques

The crystal structure of the prepared samples were studied using a X-ray diffractometer (Philips PANalytical X'PERT-PRO) with  $\text{CuK}\alpha$  radiation ( $\lambda = 1.541 \text{ \AA}$ ) at room temperature and  $1^\circ$  per min scanning speed in a range of  $2\theta$  from  $20$  to  $60^\circ$ . The lattice parameters were calculated from the X-ray diffraction (XRD) data. The microstructure of the sintered samples was examined by a Field Emission Scanning Electron Microscopy (FESEM, model no. JEOL JSM 7600F). The X-ray density ( $\rho_x$ ) of the samples was determined by the formula,  $\rho_x = \frac{n \times M_A}{N_A V}$ , where,  $n$  is the number of atoms in a unit cell,  $M_A$  is the molar mass of the sample,  $N_A$  is the Avogadro's number and  $V$  is the volume of the unit cell. The bulk density ( $\rho_B$ ) of each sample was calculated using the relation:  $\rho_B = \frac{m}{\pi r^2 d}$ , where,  $m$  is the mass,  $r$  is the radius and  $d$  is the thickness of the sample. The dielectric measurements were carried out at room temperature within the frequency range of  $1 \text{ kHz} - 1 \text{ MHz}$  by using an Impedance Analyzer (Wayne Kerr 6500B). To measure dielectric properties ( $\epsilon'$  and  $\tan \delta_E$ ) the samples were painted on both sides by conducting silver paste to ensure good electrical contacts. The  $\sigma_{AC}$  of the samples was calculated using the relation:  $\sigma_{AC} = \omega \epsilon' \epsilon_0 \tan \delta_E$ , where,  $\omega$  is the angular frequency and  $\tan \delta_E$  is the dielectric loss. The magnetic hysteresis loops (M-H loops) were measured using a vibrating sample magnetometer (VSM) (Micro Sense, EV9). The real part ( $\mu_i'$ ) and imaginary part ( $\mu_i''$ ) of the complex initial permeability ( $\mu_i^*$ ) were measured as a function of frequency within the range of  $10 \text{ kHz}$  to  $100 \text{ MHz}$  using a Wayne Kerr 6500B Impedance Analyzer. The ME effect was obtained by applying an AC magnetic field superimposed on a dc magnetic field on the sample and then measuring the output signal with applied dc magnetic field. An electromagnet was used to provide a dc magnetic field up to  $0.77 \text{ T}$ . A signal generator operating at a frequency of  $50 \text{ Hz}$  was used to drive the Helmholtz coil to generate an AC magnetic field. The output voltage generated from the sample under



investigation was measured using a Keithley multimeter (Model 2000) as a function of dc magnetic field. Details of the measurement techniques are given below:

### 3.2.1 X-ray diffraction

X-ray diffraction (XRD) is a versatile non-destructive analytical technique for identification and quantitative determination of various crystalline phases of powdered and solid sample of any compound. Bragg reflection is a coherent elastic scattering in which the energy of the X-ray is not changed on reflection. If a beam of monochromatic radiation of wavelength  $\lambda$  is incident on a periodic crystal plane at an angle  $\theta$  and is diffracted at the same angle as shown in Fig. 3.4, the Bragg's diffraction condition for X-rays is given by,

$$2d \sin\theta = n\lambda \quad (3.2)$$

where,  $d$  is the distance between crystal planes and  $n$  is the positive integer which represents the order of reflection. Eq. (3.2) is known as Bragg's law. This Bragg's law

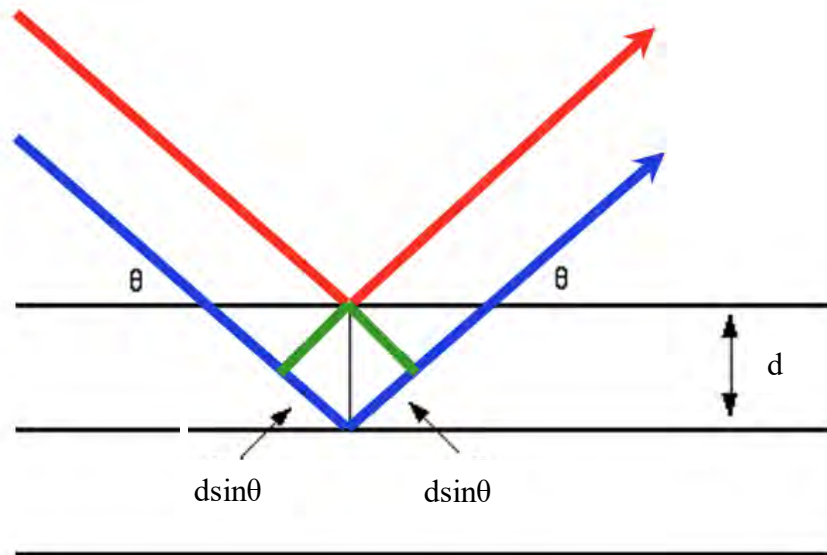


Fig. 3.4 Bragg's diffraction for X-ray.

suggests that the diffraction is only possible when  $\lambda \leq 2d$ . For this reason the visible light cannot be used to determine the crystal structure of a material. The XRD provides substantial information on the crystal structure.

XRD is carried out with a X-ray diffractometer for all categories of perovskite and composites. For this purpose monochromatic  $\text{CuK}\alpha$  radiation is used. The lattice parameter for each peak of each sample is calculated by using the formula of the crystal structure.

### 3.2.2 Scanning electron microscopy

The scanning electron microscopy (SEM, Fig. 3.5) is a type of electron microscope that images the sample surface by scanning it with a high-energy beam of electrons. It consists of an electron optical column, a vacuum system and various electronics. The electron gun at the top of the column produces a high-energy electron beam, which is focused into a fine spot ( $< 4$  nm in diameter) on the specimen. Secondary electrons are produced on the specimen surface and are detected by a suitable detector. The amplitude of the secondary electron signal varies with time according to the topography of the specimen surface. Then the signal is amplified and used to display the corresponding specimen information.

In the SEM, the magnification is totally determined by the electronic circuitry that scans the beam over the specimen's surface. Magnification can be as high as  $300,000\times$ . In principle, the resolution of a SEM is determined by the beam diameter on the surface of the specimen. However, the practical resolution depends on the properties of the specimen, the specimen preparation technique and also on many instrumental parameters, such as the beam intensity, accelerating voltage, scanning speed, distance of the lens from the specimen's surface and the angle of the specimen with respect to the detector. Under optimum conditions, a resolution of 1 nm can be achieved.

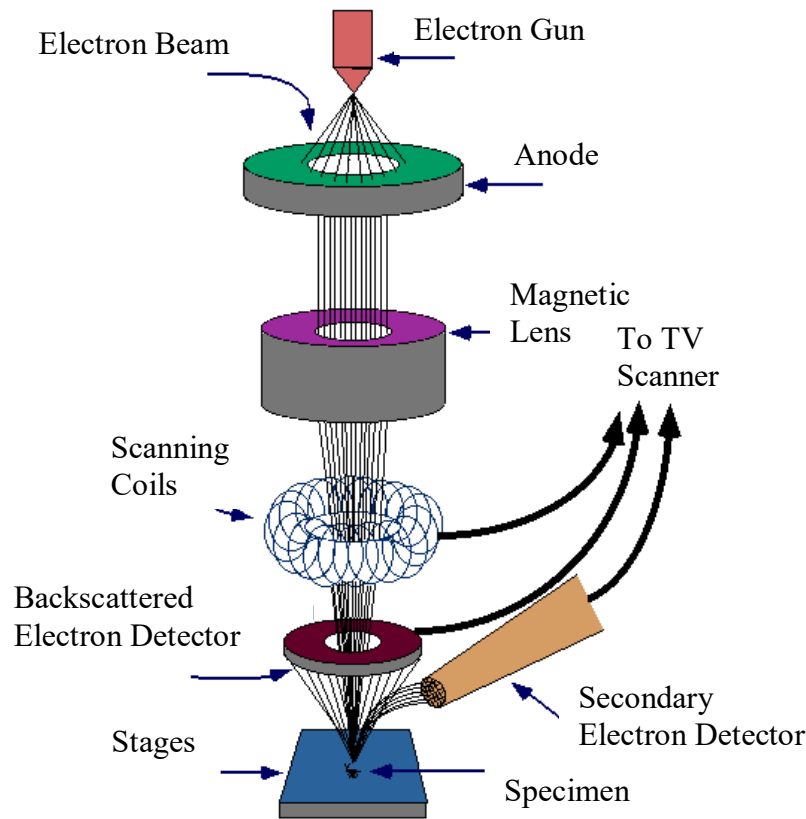


Fig. 3.5 Schematic diagram of Scanning Electron Microscope.

### 3.2.3 Energy dispersive X-ray spectroscopy

Energy dispersive X-ray spectroscopy (EDX) is an analytical technique used for the elemental analysis or chemical characterization of a sample. It is one of the variants of X-ray fluorescence spectroscopy, which relies on the investigation of a sample through interactions between electromagnetic radiation and matter, analyzing X-rays that are characteristics of an element's atomic structure to be identified uniquely from one another.

An EDX system is comprised of three basic components, the X-ray detector, the pulse processor and the analyzer, that must be designed to work together to achieve optimum results. In practice, the X-ray detector first detects and converts X-rays into electronic signals. Then, the pulse processor measures the electronic signals to determine the energy of each X-ray detected. Finally, the analyzer displays and interprets the X-ray data.

In the present work, compositional analyses were performed by using the EDX system attached with the JEOL-7600 FESEM.

### 3.2.4 Dielectric measurements

The dielectric properties, AC conductivity etc. were measured using Wayne Kerr Impedance Analyzer 6500B series. Experimental set up is shown in Fig. 3.6.

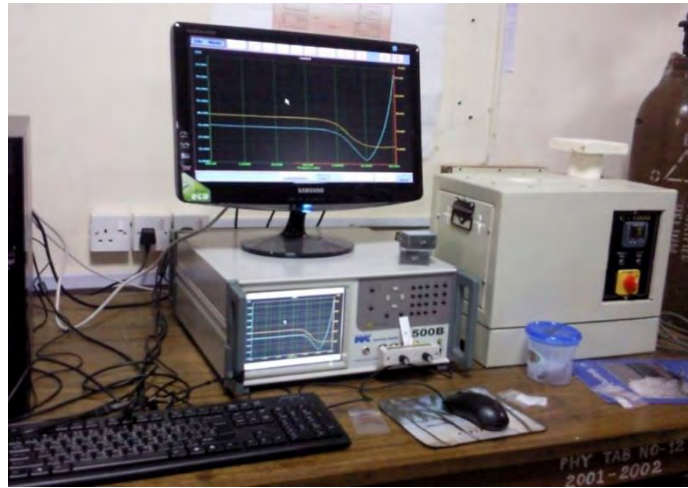


Fig. 3.6 Wayne Kerr impedance analyzer 6500B series.

Measurements of dielectric properties normally involve the measurements of the change in capacitance and loss of a capacitor in presence of the dielectric materials. The behavior of a capacitance can now be described as follows. An ideal loss less air capacitor of capacitance  $C_0$  is considered. On insertion of a dielectric material in air space the capacitance are changed. The value of  $\epsilon'$  and electrical properties (AC conductivity and impedance) measurements on disk-shaped specimens are carried out at room temperature on all the samples in the high frequency range. The values of  $\epsilon'$  are calculated using the following relations,

$$\epsilon' = \frac{C}{C_0} \text{ and } \epsilon'' = \epsilon' \tan \delta_E, \quad (3.3)$$

where,  $C$  is the capacitance of the sample and

$$C_0 = \frac{\varepsilon_0 A}{d} \text{ is derived geometrically-} \quad (3.4)$$

is the capacitance of the capacitor without the dielectric materials,  $d$  is the thickness of the capacitor and  $A (= \pi r^2)$  is the area of cross section of the disk shape sample.

The  $\sigma_{AC}$  is determined at room temperature in the frequency range 20 Hz – 1 MHz to study the mechanism of conduction. The  $\sigma_{AC}$  of the sample is calculated from the dielectric data using the relation,

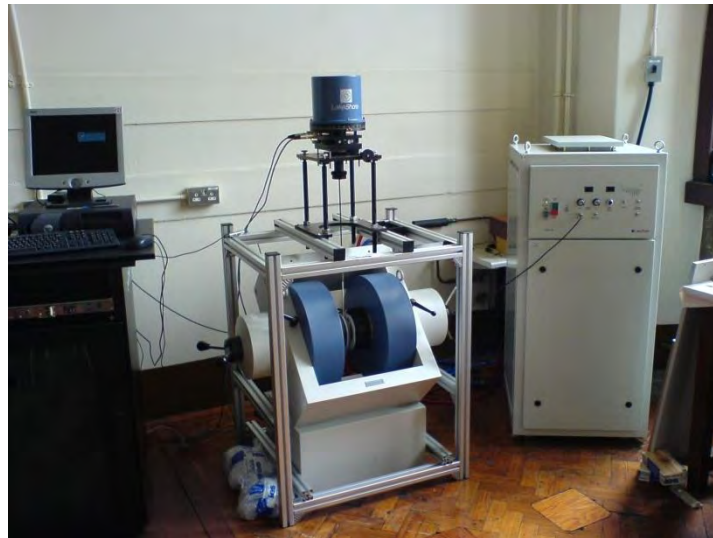
$$\sigma_{AC} = \omega \varepsilon' \varepsilon_0 \tan \delta_E \quad (3.5)$$

where,  $\varepsilon'$  is the dielectric constant,  $\varepsilon_0 (= 8.85 \times 10^{-12} \text{ F m}^{-1})$  is the permittivity of free space,  $\omega$  is the angular frequency and  $\tan \delta_E$  is the dielectric loss.

### 3.2.5 Magnetic Properties

#### 3.2.5.1 M-H hysteresis loops

Dependence of magnetization on external magnetic field e.g. M-H curves for the materials were measured using Vibrating Sample Magnetometer (VSM). Measurement set up



**Fig. 3.7** The Lakeshore vibrating sample magnetometer.

is shown in Fig. 3.7. The sample is placed inside a uniform magnetic field to be magnetized and vibrating the sample sinusoidally, the induced voltage due to the magnetic moment in the pickup coil is proportional to the samples magnetization. Therefore by detecting the induced voltage, it is possible to measure the magnetic field-dependent magnetization hysteresis curve of the materials.

### 3.2.5.2 Complex initial permeability

The complex initial permeability ( $\mu_i^*$ ), magnetic loss tangent ( $\tan \delta_M$ ), quality factor are measured using the Wayne Kerr Impedance analyzer 6500B series. Toroid shaped samples (Fig. 3.8) are used for the measurement of complex permeability at room temperature in the frequency range 1 kHz - 120 MHz. The value of  $\mu_i'$  and  $\mu_i''$  are calculated using the relations:  $\mu_i' = L_s/L_0$  and  $\mu_i'' = \mu_i' \tan \delta_M$ , where  $L_s$  is the self-inductance of the sample core and  $L_0 = \mu_o N^2 S/\pi \bar{d}$  is derived geometrically. Here,  $L_0$  is the inductance of the



**Fig. 3.8** Toroid shaped sample for permeability measurement.

winding coil without the sample core;  $N$  is the number of turns of the coil ( $N = 5$ ),  $S$  is the area of cross section of the toroidal sample as given below:

$$S = d \times h, \quad (3.9)$$

where, 
$$d = \frac{d_2 - d_1}{2}, \quad (3.10)$$

$d_1$  = Inner diameter,

$d_2$  = Outer diameter,

$h$  = Height

and  $\bar{d}$  is the mean diameter of the toroidal sample as given below:

$$\bar{d} = \frac{d_1 + d_2}{2} \quad (3.11)$$

The relative quality factor (RQF) is determined from the ratio  $\frac{\mu_i'}{\tan \delta_M}$ .

### 3.2.6 Magnetolectric coefficient

Fig. 3.9 shows the experimental setup for the measurement of ME coefficient. To measure the ME coefficient the sides of the pellet is connected with a Keithley 2000 microvoltmeter that gives the value of output voltage. The sample is then

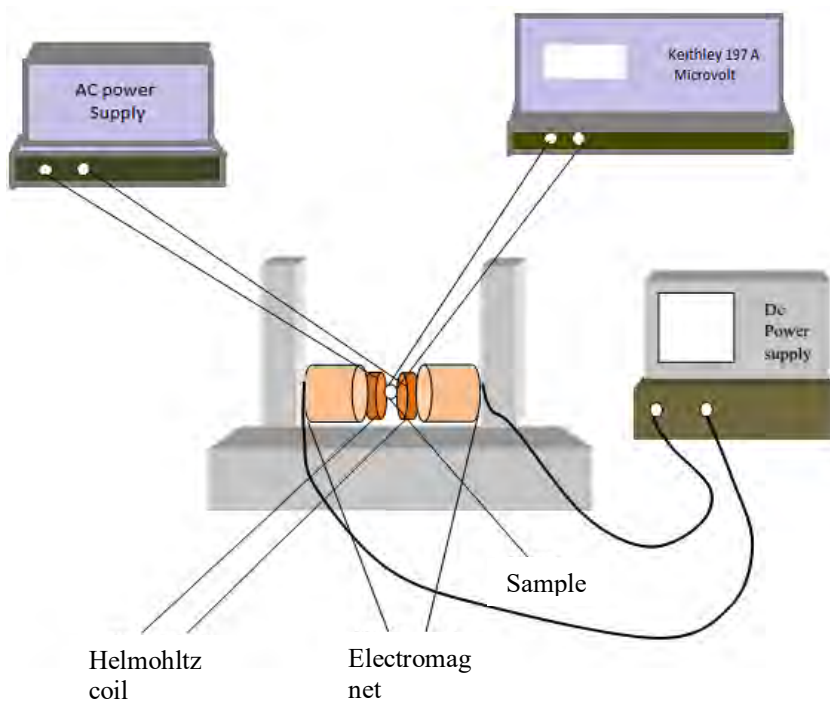


Fig. 3. 9. Experimental setup for the measurement of magnetolectric coefficient.

placed between two faces of an electromagnet. Here another pair of coil called Helmholtz-coil is placed vertically and parallel to the faces of electromagnet. The Helmholtz coil is connected to an AC power supply and create AC magnetic field. The sides of electromagnet are connected with a dc power supply. By changing current and voltage from dc power supply magnetic field is changed of the electromagnet and the sample experience different magnetic condition. Hence output voltage is changed. ME coefficient ( $\alpha_{ME}$ ) has been calculated using the relation,

$$\alpha_{ME} = \left( \frac{dE}{dH} \right)_{H_{AC}} = \frac{V_o}{h_o d}, \quad (3.12)$$

where,  $V_o$  is the ME voltage across the sample surface and  $h_o$  is the amplitude of the AC magnetic field and  $d$  is the thickness of the sample.



**References**

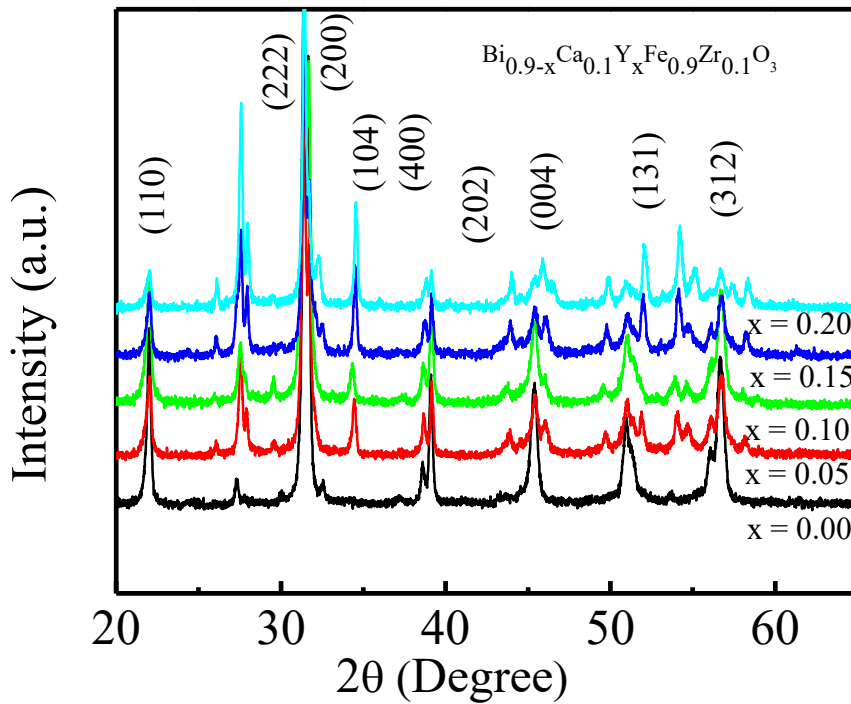
- [1] Moulson, A. J. and Herbert, J. M., "Electroceramics: materials, properties and application", *Chapman & Hall, UK*, 1990.
- [2] Xu, Y., "Ferroelectric materials and their applications", *Elsevier Science Pub. Co., New York, USA*, 1991.
- [3] Fang, J., Wang, J., Gan, L. M. and Ng, S. C., "Comparative study of phase development of lead titanate powders", *Mater. Lett.*, Vol. 52, pp. 304-312, 2002.
- [4] Wodecka, D. B. and Czekey, D., "Synthesis of  $0.7\text{BiFeO}_3-0.3\text{BaTiO}_3$  ceramics: thermal, structural and ac impedance studies", *Archives of Metallurgy and Materials*, Vol. 56, pp. 1127-1136, 2011.
- [5] Coble, R. L. and Burke, J. E., "On the reactivity of solids", *4<sup>th</sup> Int. Symp.*, 30 May-4 June, Amsterdam, pp. 38-51, 1960.
- [6] MacDonald, J. R., "Impedance spectroscopy", *Wiley-Interscience, New York*, 1987.

## Chapter 4

## RESULTS AND DISCUSSION

## 4.1 X ray diffraction analysis

The XRD patterns of  $\text{Bi}_{0.9-x}\text{Ca}_{0.1}\text{Y}_x\text{Fe}_{0.9}\text{Zr}_{0.1}\text{O}_3$  sintered at  $910^\circ\text{C}$  is shown in Fig.4.1. The compound  $\text{BiFeO}_3$  had a rhombohedrally distorted perovskite structure with space group R3c at room temperature.



**Fig. 4.1** X-ray diffraction of  $\text{Bi}_{0.9-x}\text{Ca}_{0.1}\text{Y}_x\text{Fe}_{0.9}\text{Zr}_{0.1}\text{O}_3$  ( $x = 0.00, 0.05, 0.10, 0.15$  and  $0.20$ ) compositions sintered at  $910^\circ\text{C}$

However, for pure  $\text{BiFeO}_3$  bulk ceramics, some previous researches indicated that the impurity phases, e.g.  $\text{Bi}_2\text{Fe}_4\text{O}_9$ , could be formed during the high-temperature sintering and binary or ternary solid solution of  $\text{BiFeO}_3$  could prevent the formation of second phase [11, 13, 14]. As shown in Figure 4.1, in the pure  $\text{BiFeO}_3$  ceramic sample, besides  $\text{BiFeO}_3$  with

R3c structure, an obvious second phase  $\text{Bi}_2\text{Fe}_4\text{O}_9$  can be observed. Once Y substituted at the Bi site, the phase  $\text{Bi}_2\text{Fe}_4\text{O}_9$  cannot be observed. However, with increasing Y content, another phase  $\text{Y}_3\text{Fe}_5\text{O}_{12}$  appears in the  $x=0.05, 0.10, 0.15$  and  $0.20$  ceramic samples.

**Table 4.1:** The lattice parameters of  $\text{Bi}_{0.9-x}\text{Ca}_{0.1}\text{Y}_x\text{Fe}_{0.9}\text{Zr}_{0.1}\text{O}_3$  compositions sintered at  $910^\circ\text{C}$ .

Y content, x	Lattice Parameters ( $\text{\AA}$ )		
	a ( $\text{\AA}$ )	b ( $\text{\AA}$ )	c ( $\text{\AA}$ )
0.00	5.0988	5.0988	8.7693
0.05	5.1291	5.1291	8.5726
0.10	5.1311	5.1311	8.6359
0.15	5.1304	5.1304	8.5008
0.20	5.1299	5.1299	8.4081

## 4.2 Density and Porosity

The X-ray density of the composition was calculated using the relation:

$$\rho_x = \frac{nM}{N_A V} \quad (4.1)$$

Where,  $n$  is the number of atoms per unit cell,  $M$  is the molecular weight of  $\text{Bi}_{0.9-x}\text{Ca}_{0.1}\text{Y}_x\text{Fe}_{0.9}\text{Zr}_{0.1}\text{O}_3$  ( $x = 0.00, 0.05, 0.10, 0.15$  and  $0.20$ ),  $N_A$  is the Avogadro's number ( $6.023 \times 10^{23}$ ) and  $V$  is the volume of unit cell.

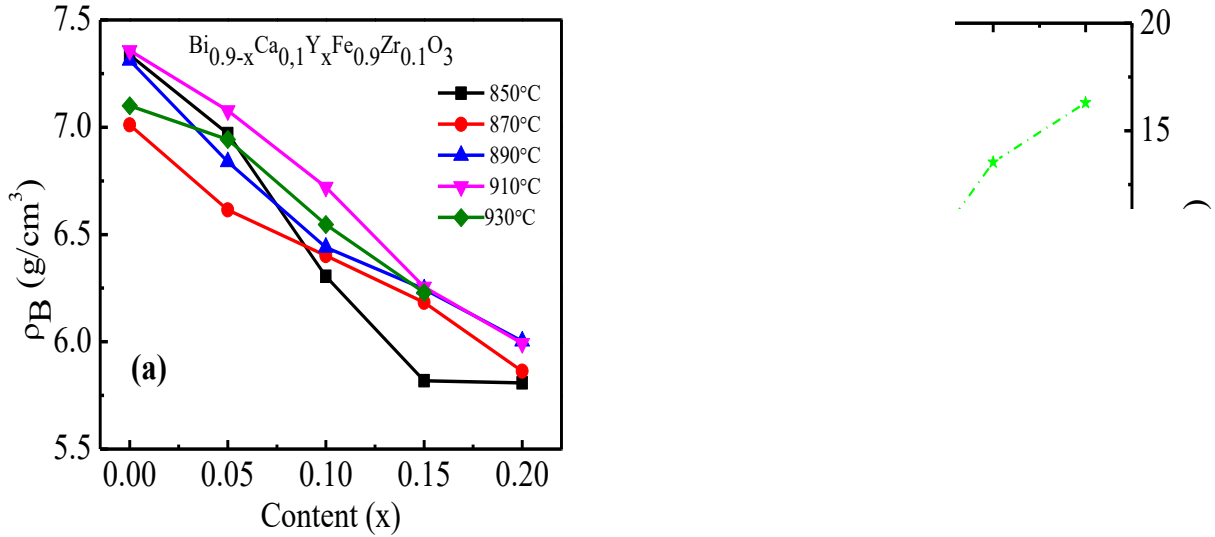
The bulk density was calculated using the formula:

$$\rho_B = \frac{m}{\pi r^2 d} \quad (4.2)$$

where  $m$ ,  $r$  and  $d$  are the mass, radius and thickness of the pellet samples, respectively.

Fig. 4.2(a) shows the variation of bulk density of the studied samples which increases with increase in sintering temperature up to a certain value and then decreases. The maximum density is found for the sintering temperature ( $T_s$ ) of  $910^\circ\text{C}$  except  $x=0.20$ . So  $910^\circ\text{C}$  is taken as an optimum  $T_s$  for our studied compositions. The bulk density increases with sintering temperature because during the sintering process the thermal energy generates a force that drives the grain boundaries to grow over the pores. Fig. 4.2(b) shows the variation of bulk density, X-ray density and porosity of the compositions for the optimum  $T_s$ . From Fig. 4.2(b), it is seen that X-ray density ( $\rho_x$ ) and bulk density decreases with the increase in Y content but bulk density of all samples is lower than X-ray density. This may be due to the existence of some pores in the bulk samples which are formed and developed during the preparation of samples or sintering process. The density decreases with the increase in Y content because the ionic radius of Y is smaller than Bi, this causes volume of the unit cell decreases. The porosity in ceramic samples develops from two sources: inter-granular porosity and intra-granular porosity [7]. Thus the total porosity (P) can be written as

$P = P_{\text{inter}} + P_{\text{intra}}$ . The bulk density decreases with the increase in Y content might be due to the increase of the intragranular pores.



**Fig. 4.2** (a) Variation of  $\rho_B$  with Y content for various sintering temperature (b) Variation of  $\rho_x$ ,  $\rho_B$  and porosity with Y content.

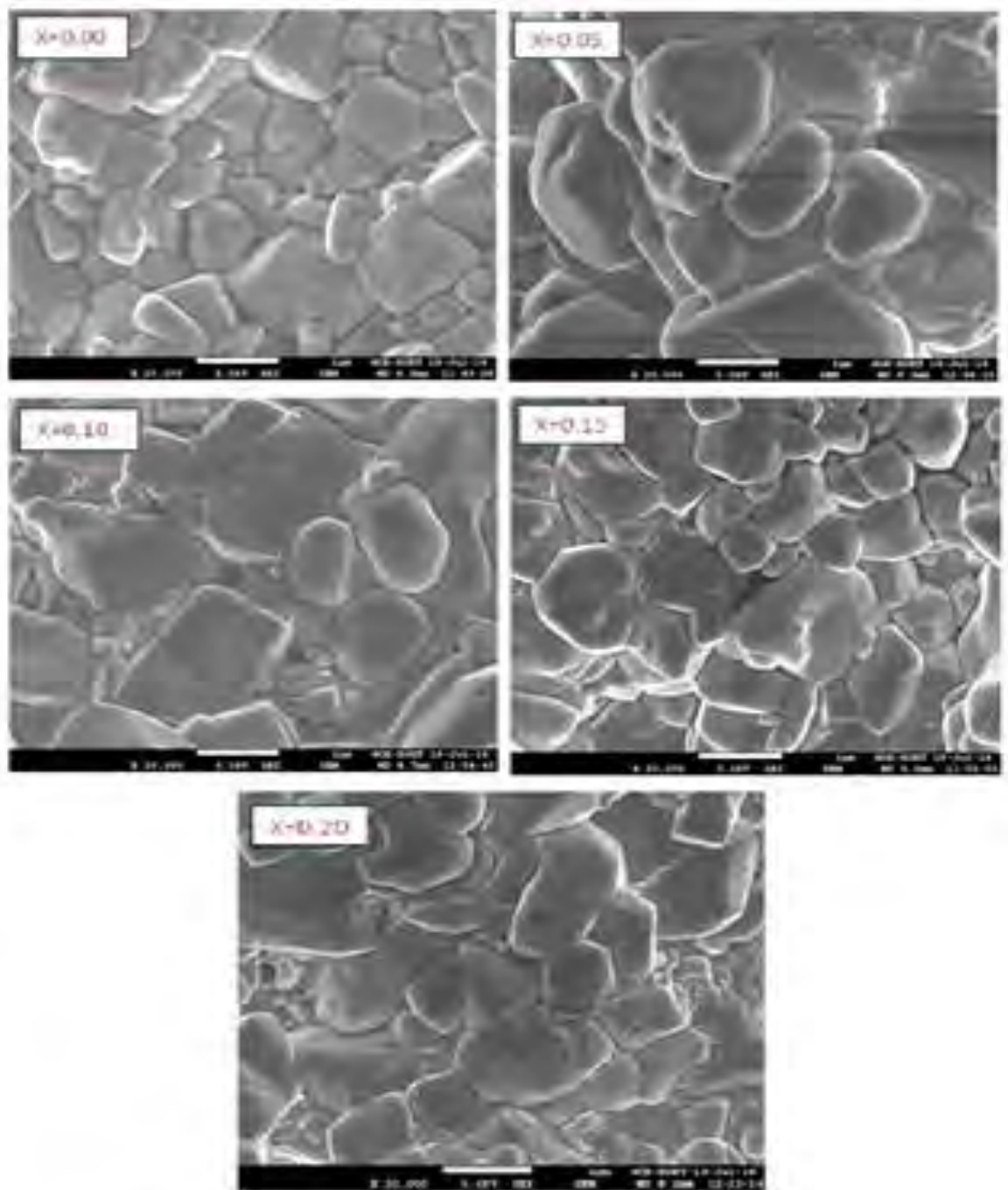
**Table 4.2** X-ray density, bulk density and porosity of various  $\text{Bi}_{0.9-x}\text{Ca}_{0.1}\text{Y}_x\text{Fe}_{0.9}\text{Zr}_{0.1}\text{O}_3$  samples sintered at 910°C.

Y content x	$\rho_x$ ( $\text{g/cm}^3$ )	$\rho_B$ ( $\text{g/cm}^3$ )	P (%)
0.00	7.957	7.357	8
0.05	7.485	7.078	5
0.10	7.272	6.721	8
0.15	7.235	6.256	14
0.20	7.160	5.993	16

### 4.3 Microstructural Analysis

The Field Emission Scanning Electron Micrographs of  $\text{Bi}_{0.9-x}\text{Ca}_{0.1}\text{Y}_x\text{Fe}_{0.9}\text{Zr}_{0.1}\text{O}_3$  sintered at 850, 890 and 910°C are shown in Fig. 4.3(a-c). Substitution of Yttrium (Y) has a significant effect on the grain size of the compositions. From the above mentioned figures it is seen that

the grain size increases with increase of sintering temperature. Irregular grain growth is occurred with Y content. The average grain size was calculated using the linear intercept technique [9]. The average grain size of  $\text{Bi}_{0.9-x}\text{Ca}_{0.1}\text{Y}_x\text{Fe}_{0.9}\text{Zr}_{0.1}\text{O}_3$  compositions with  $T_s$  is shown in Table 4.3.



**Fig. 4.3(a)** The microstructure of various  $\text{Bi}_{0.9-x}\text{Ca}_{0.1}\text{Y}_x\text{Fe}_{0.9}\text{Zr}_{0.1}\text{O}_3$  samples sintered at  $850^\circ\text{C}$ .

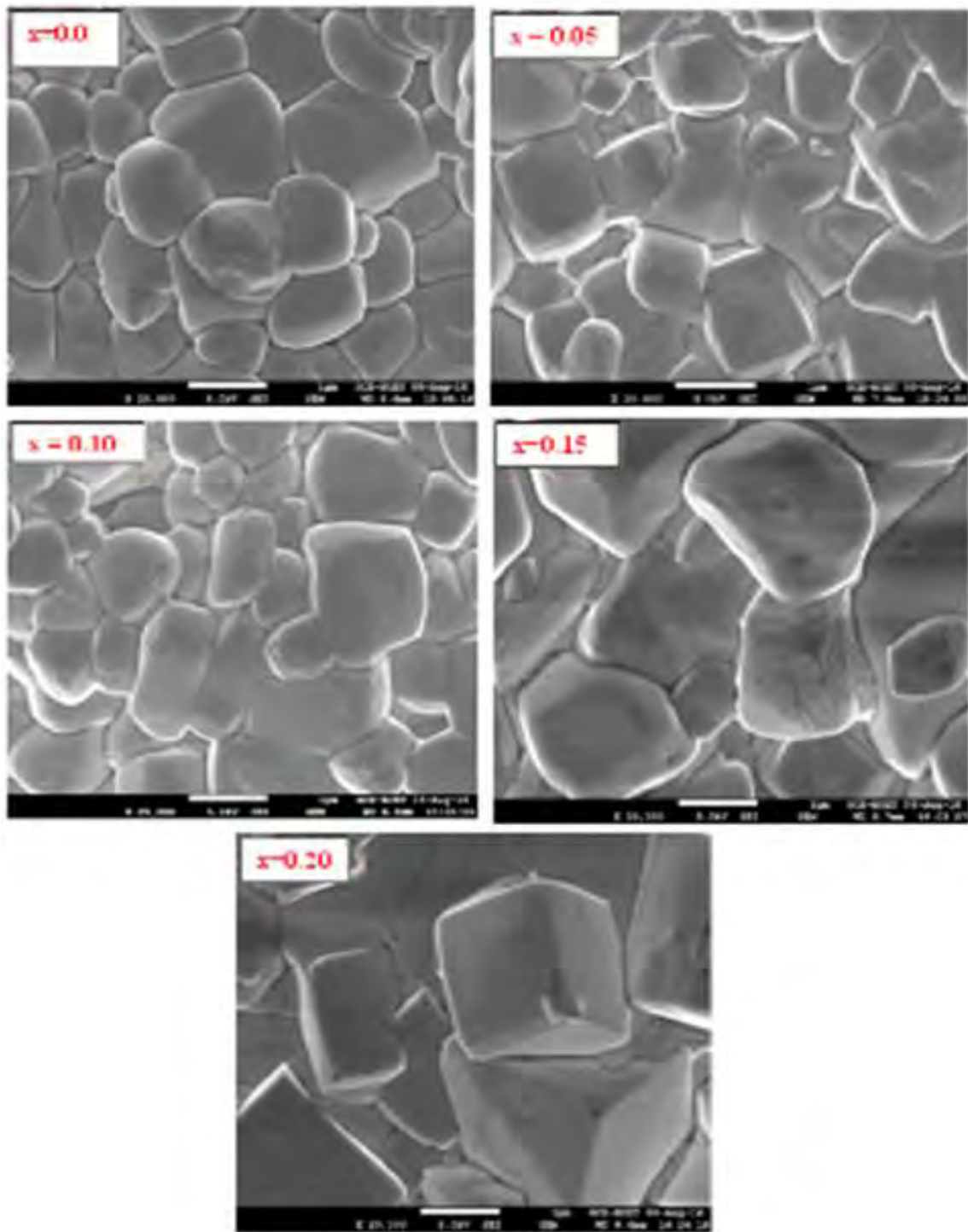


Fig. 4.3(b) The microstructure of various  $\text{Bi}_{0.9-x}\text{Ca}_{0.1}\text{Y}_x\text{Fe}_{0.9}\text{Zr}_{0.1}\text{O}_3$  samples sintered at  $910^\circ\text{C}$ .

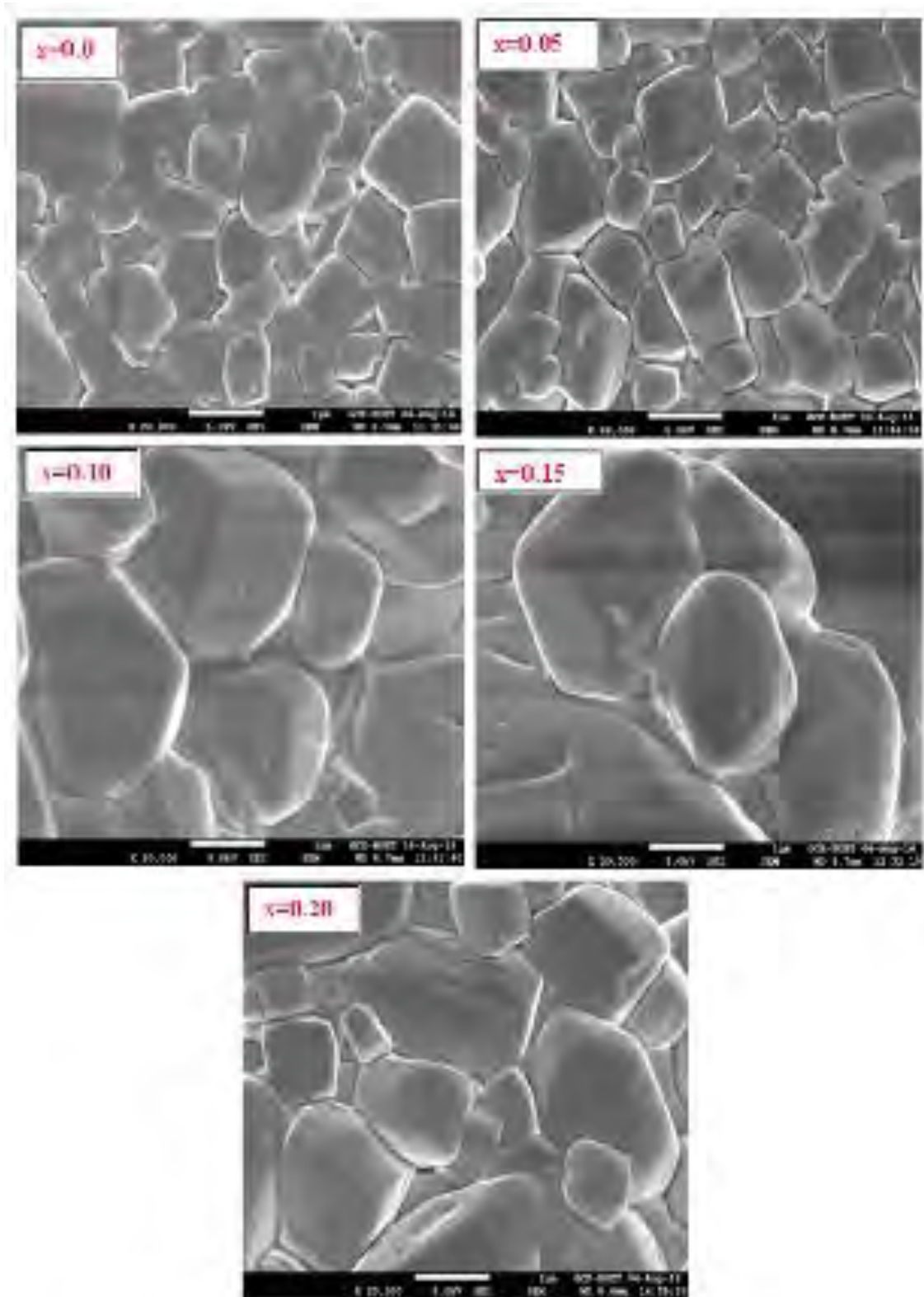


Fig. 4.3(c) The microstructure of various  $\text{Bi}_{0.9-x}\text{Ca}_{0.1}\text{Y}_x\text{Fe}_{0.9}\text{Zr}_{0.1}\text{O}_3$  samples sintered at  $930^\circ\text{C}$ .



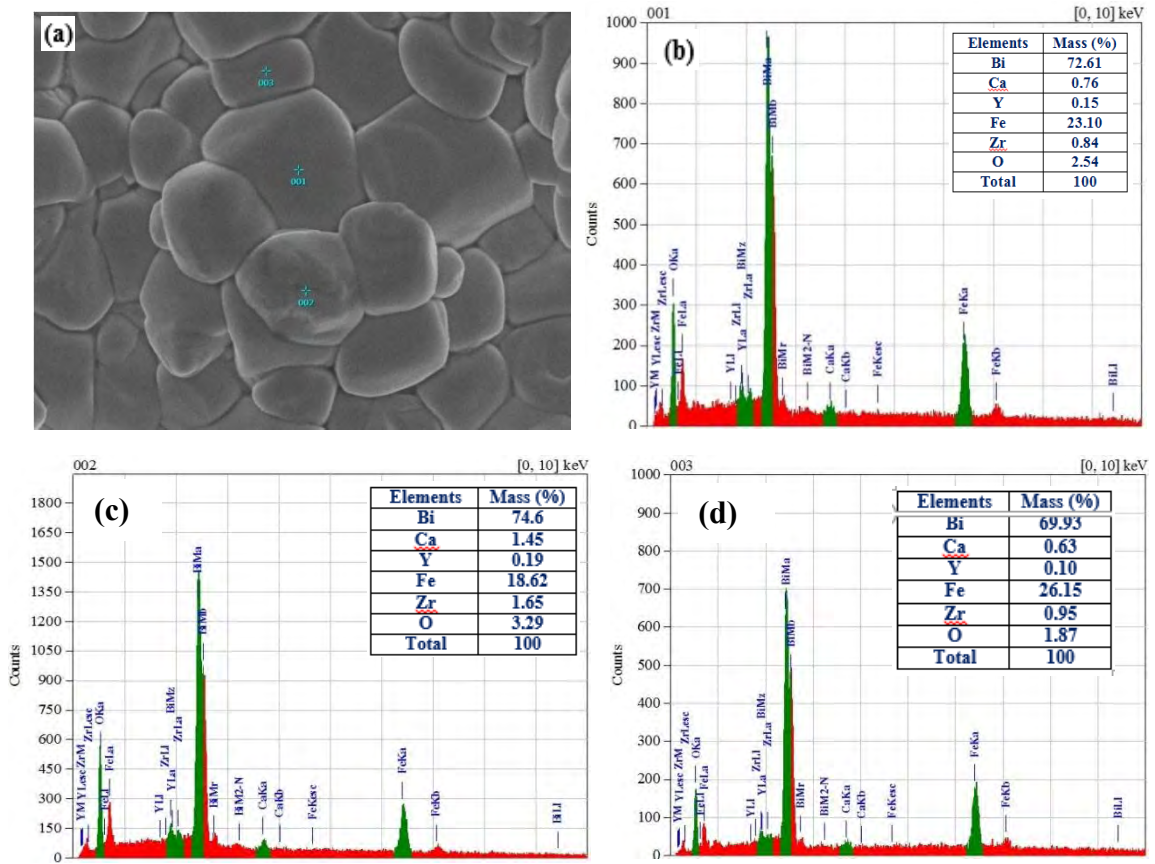
**Table 4.3:** Average grain size of the compositions  $\text{Bi}_{0.9-x}\text{Ca}_{0.1}\text{Y}_x\text{Fe}_{0.9}\text{Zr}_{0.1}\text{O}_3$  sintered at 850, 910 and 930 °C.

$T_s$	Average grain size ( $\mu\text{m}$ )				
	x=0.00	x=0.05	x=0.10	x=0.15	x=0.20
850 °C	1.0976	0.9435	0.7503	1.1388	0.9978
910 °C	1.1381	1.4370	1.4792	1.5862	1.6896
930 °C	1.0238	1.0672	1.3619	1.4394	1.5189

#### 4.4 Energy Dispersive X-ray Spectroscopy Analysis

Energy dispersive X-ray spectra (EDS) of various  $\text{Bi}_{0.9-x}\text{Ca}_{0.1}\text{Y}_x\text{Fe}_{0.9}\text{Zr}_{0.1}\text{O}_3$  ( $x = 0.00-0.20$ ) ceramics recorded from FESEM to determine the chemical composition. The percentages of elements present in compositions are listed in the attached table of EDS spectra. The EDS spectra have also been taken at different points of the samples to provide quantitative elemental analysis as given in Fig 4.4.1 (a-e).

EDS confirms the Y doping in the compositions. EDS spectroscopy also confirms homogeneous distribution of the constituent elements. It is also confirmed that Y concentration increased at the grain boundaries with increasing sintering temperature.



**Fig. 4.4.1** (a) Image used for EDS study. EDS spectra of (b) point 1, (c) point 2 and (d) point 3 of  $\text{Bi}_{0.9}\text{Ca}_{0.1}\text{Fe}_{0.9}\text{Zr}_{0.1}\text{O}_3$  samples sintered at  $910^\circ\text{C}$ .

**Table 4.4.1:** Calculated % of mass of elements in  $\text{Bi}_{0.9}\text{Ca}_{0.1}\text{Fe}_{0.9}\text{Zr}_{0.1}\text{O}_3$  ( $x=0.0$ ) samples sintered at  $910^\circ\text{C}$ .

Composition	Elements	Calculated % of mass
$\text{Bi}_{0.9}\text{Ca}_{0.1}\text{Fe}_{0.9}\text{Zr}_{0.1}\text{O}_3$ (x=0.0)	Bi	62.805
	Ca	1.3383
	Fe	16.783
	Zr	3.046
	O	16.028

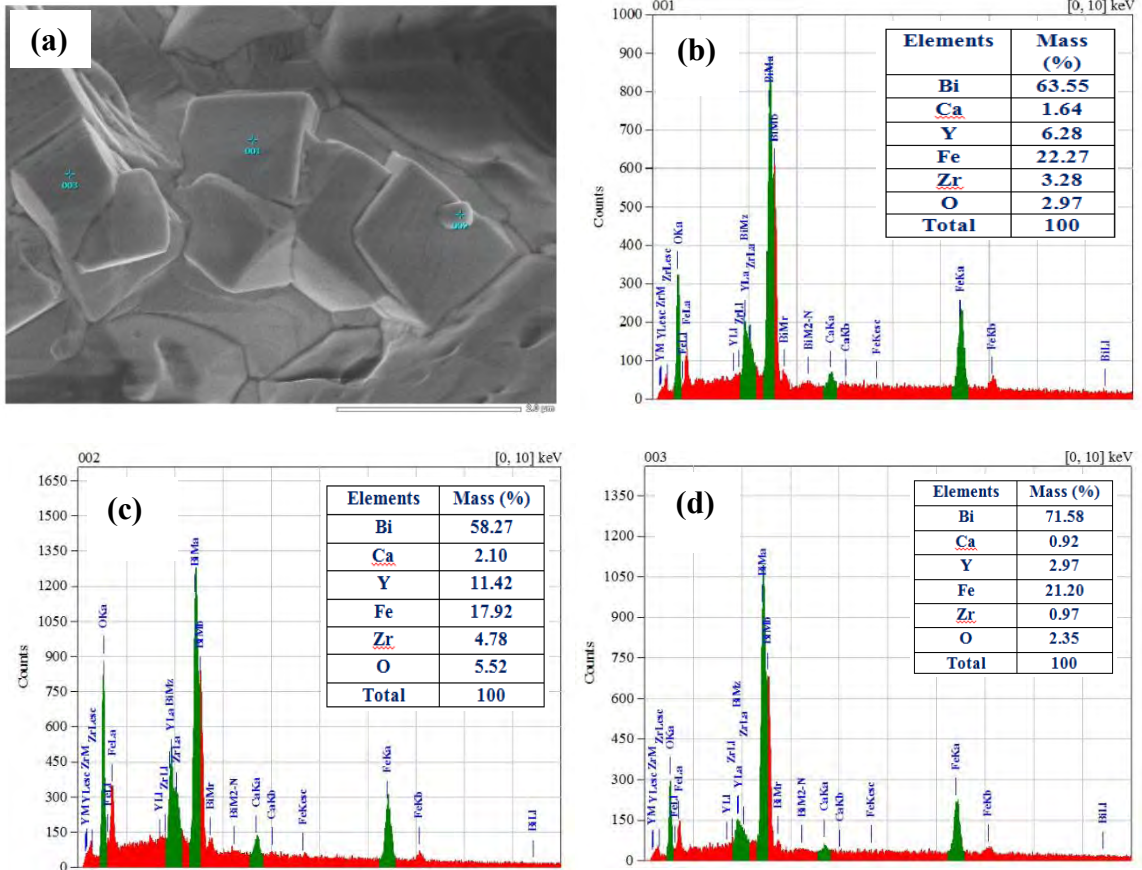


Fig. 4.4.2 (a) Image used for EDS study. EDS spectra of (b) point 1, (c) point 2 and (d) point 3 of  $\text{Bi}_{0.7}\text{Ca}_{0.1}\text{Y}_{0.2}\text{Fe}_{0.9}\text{Zr}_{0.1}\text{O}_3$  samples sintered at 910°C.

Table 4.4.2: Calculated % of mass of elements in  $\text{Bi}_{0.7}\text{Ca}_{0.1}\text{Y}_{0.2}\text{Fe}_{0.9}\text{Zr}_{0.1}\text{O}_3$  (x=0.2) samples sintered at 910°C.

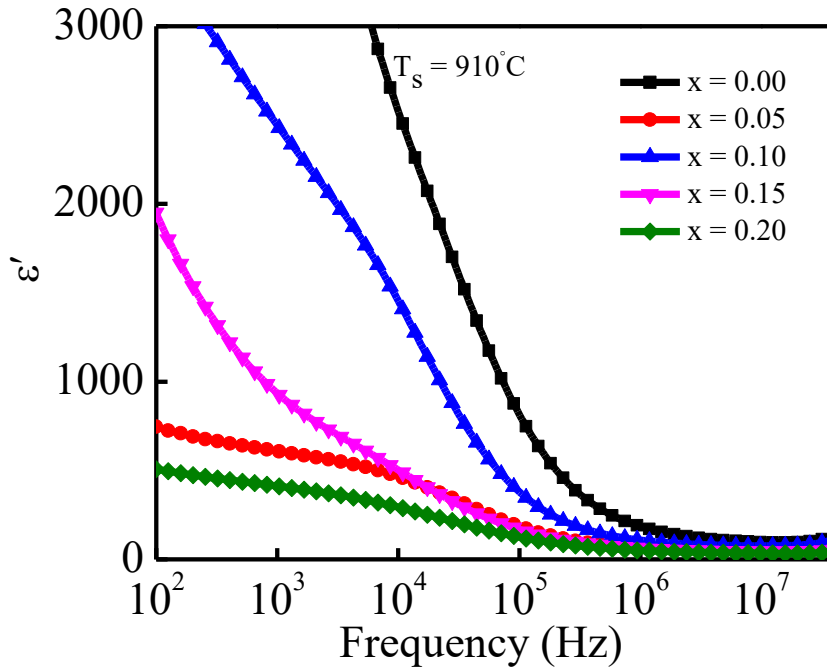
Composition	Elements	Calculated % of mass
$\text{Bi}_{0.7}\text{Ca}_{0.1}\text{Y}_{0.2}\text{Fe}_{0.9}\text{Zr}_{0.1}\text{O}_3$ (x=0.2)	Bi	53.107
	Ca	1.455
	Y	6.455
	Fe	18.246
	Zr	3.312
Total		17.425
		100.00

## 4.5 Dielectric Properties

### 4.5.1 Real part of dielectric constant

Fig. 4.5 shows the frequency dependent dielectric constant ( $\epsilon'$ ) of various  $\text{Bi}_{0.9-x}\text{Ca}_{0.1}\text{Y}_x\text{Fe}_{0.9}\text{Zr}_{0.1}\text{O}_3$  compositions measured at room temperature. From Fig 4.5, a decreasing trend is found with frequency increasing from 100 Hz to 10 MHz is observed in all samples. The phenomenon of dipole relaxation process helps us to explain this observation that is dipoles are able to tag along the frequency of the applied field at low frequencies, at the same time as they are unable to follow the frequency of the applied field at high frequencies [6]. In addition different types of polarizations like dipolar, interfacial, ionic and electronic polarizations contribute to the dielectric constant at low frequency. But as the frequency increase beyond a certain limit, dipoles are unable to make themselves parallel with the applied electric field and contribution from different polarizations decreases. At higher frequency the dielectric constant totally depend only on electronic polarization and consequently the dielectric constant decrease. The sharp decrease in the values of at lower frequencies can be explained on the basis of Maxwell-Wagner two layer model [7] in accord with Koop's phenomenon theory [8]. Accordingly, the dielectric structure of a material is made up of well conducting layer of grains followed by poorly conducting layer of grain boundaries. The high value of dielectric constant comes from the space charge polarization produced at the grain boundary. The polarization mechanism involves the exchange of electrons between the ions of the same element, which are present in more than one valance state and are distributed randomly over randomly over crystallographic equivalent sites. Here the exchange of the electrons mainly takes place between  $\text{Fe}^{3+}$ - $\text{Fe}^{2+}$  present at octahedral sites (B-site). During this exchange mechanism the electrons have to pass through the grains and grain boundary of the dielectric medium. Owing to high resistance of the grain boundary, the electrons accumulate at grain boundary and produce space charge polarization. It is well

known that the grain boundaries are more effective at low frequency and grains are effective at high frequency [8, 9].



**Fig.4.5** Frequency dependent real part of complex dielectric constant of various  $\text{Bi}_{0.9-x}\text{Ca}_{0.1}\text{Y}_x\text{Fe}_{0.9}\text{Zr}_{0.1}\text{O}_3$  sintered at  $910^\circ\text{C}$ .

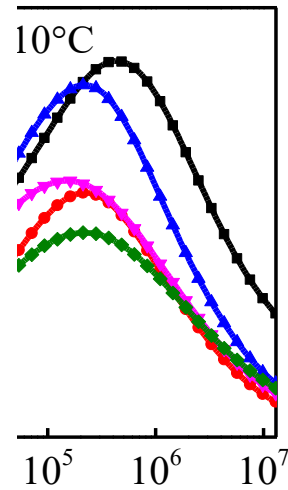
#### 4.5.2 Imaginary part of dielectric constant

Fig. 4.6 shows the variation of the  $\epsilon''$  of the compositions  $\text{Bi}_{0.9-x}\text{Ca}_{0.1}\text{Y}_x\text{Fe}_{0.9}\text{Zr}_{0.1}\text{O}_3$  sintered at different temperatures, which shows similar behavior as dielectric constant. It is observed that the  $\epsilon''$  decreases with the increase in frequency and merges at higher frequencies.

**Fig. 4.6** Frequency dependent imaginary part of complex dielectric constant of various  $\text{Bi}_{0.9-x}\text{Ca}_{0.1}\text{Y}_x\text{Fe}_{0.9}\text{Zr}_{0.1}\text{O}_3$  sintered at  $910^\circ\text{C}$ .

#### 4.5.2 Dielectric loss

Fig. 4.7 shows the variation of dielectric loss of various  $\text{Bi}_{0.9-x}\text{Ca}_{0.1}\text{Y}_x\text{Fe}_{0.9}\text{Zr}_{0.1}\text{O}_3$  compositions sintered at different temperatures. From Fig. 4.7, it can be seen that for all the samples there is a pick. This pick indicates the relaxor behavior of the compositions. The width of the pick of Y un doped sample is larger than the doped samples and at higher frequency ( $>10$  MHz) the dielectric loss is smaller of Y doped  $\text{Bi}_{0.9-x}\text{Ca}_{0.1}\text{Y}_x\text{Fe}_{0.9}\text{Zr}_{0.1}\text{O}_3$  than that of un doped  $\text{Bi}_{0.9-x}\text{Ca}_{0.1}\text{Fe}_{0.9}\text{Zr}_{0.1}\text{O}_3$ , which means the compositions could possibly be used in practical applications such as magnetically tunable filters and oscillators. This loss factor is attributed to domain wall resonance. At high frequencies, the dielectric loss is low due to the inhibition of domain wall motion. The dielectric loss is found to be maximum in the frequency range 1 kHz–1 MHz. The maximum dielectric loss is observed when the hopping frequency of electrons between different ionic sites becomes nearly equal to the frequency of the applied field [15].



**Fig. 4.7** Frequency dependent dielectric loss of various  $\text{Bi}_{0.9-x}\text{Ca}_{0.1}\text{Y}_x\text{Fe}_{0.9}\text{Zr}_{0.1}\text{O}_3$  sintered at  $910^\circ\text{C}$ .

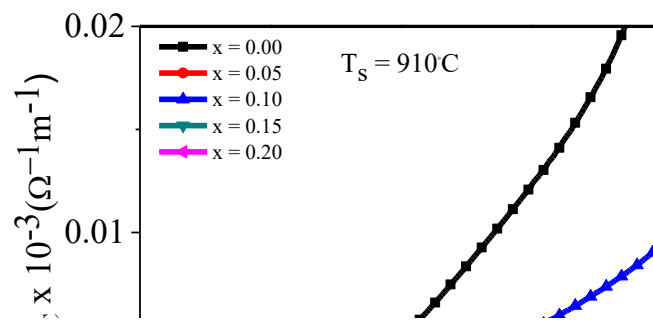
#### 4.6 AC conductivity

In the research of materials science conductivity is an important issue. Conductivity plays a crucial role in BFO [24]. BFO is one of the most extensively studied multiferroic compound which exhibits electric as well as magnetic properties at room temperature. Fig.4.8 shows the variation of AC conductivity with frequency of various  $\text{Bi}_{0.9-x}\text{Ca}_{0.1}\text{Y}_x\text{Fe}_{0.9}\text{Zr}_{0.1}\text{O}_3$  sintered at  $910^\circ\text{C}$ . At lower frequency, which corresponds to DC conductivity, the conductivity is almost independent of frequency. On the other hand, at higher frequency, which is known as hopping region; the AC conductivity ( $\sigma_{ac}$ ) increases faster than that of DC conductivity. At high frequency the conductive grains become more active and hence increases hopping of charge carriers and contribute to rise in conductivity. The frequency dependent AC conductivity of  $\text{Bi}_{0.9-x}\text{Ca}_{0.1}\text{Y}_x\text{Fe}_{0.9}\text{Zr}_{0.1}\text{O}_3$  relaxors obey the Jonscher's power law [14]. The variation of  $\sigma_{ac}$  can be explained in terms of polaron hopping mechanism [14] among the localized states. In the large polaron model,  $\sigma_{ac}$  decrease with increase of frequency, while in small polaron hopping mechanism, the  $\sigma_{ac}$  with increase of frequency [14, 22].

In present investigation, all compositions exhibit an increase in conductivity with frequency as shown in Fig. 4.9 which indicates that small polaron hopping present in the conduction mechanism of the studied compound. The variation of  $\sigma_{ac}$  can also be explained on the basis of Jonscher's law [23]:

$$\sigma_{ac}(\omega) = \sigma_{dc} + B\omega^n \quad (4.3)$$

where,  $\sigma_{ac}(\omega)$  is the total electrical conductivity,  $\sigma_{dc}$  is the frequency independent dc conductivity, B is the temperature dependent pre-exponential factor and „n“ is the frequency exponent. The exponent „n“ represents the degree of interaction between mobile ions and the lattice around them. The value of „n“ can have between 0 and 1 (<1). Both B and „n“ are temperature and material dependent [24]. The values of n are calculated from the slope of the fitting the data for each composition. Thus the conduction process in the present composition is mainly due to small polaron hopping. According to Jonscher's law the variation of  $\log(\sigma_{ac})$  with  $\log(\omega)$  should be linear. However, a slight deviation from linearity is attributed to mixed polaron (small/large) conduction. Hopping mechanism is favored in ionic lattices in which the same kind of cation is found in two different oxidation states.



**Fig. 4.8** Frequency dependent AC conductivity of various  $Bi_{0.9-x}Ca_{0.1}Y_xFe_{0.9}Zr_{0.1}O_3$  sintered at  $910^\circ C$ .



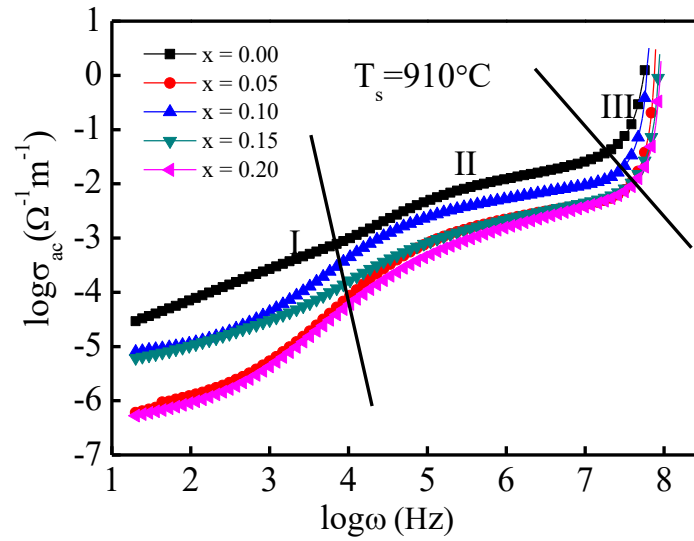


Fig. 4.9  $\log \sigma_{ac}$  vs  $\log \omega$  plot of various  $\text{Bi}_{0.9-x}\text{Ca}_{0.1}\text{Y}_x\text{Fe}_{0.9}\text{Zr}_{0.1}\text{O}_3$  sintered at  $910^\circ\text{C}$ .

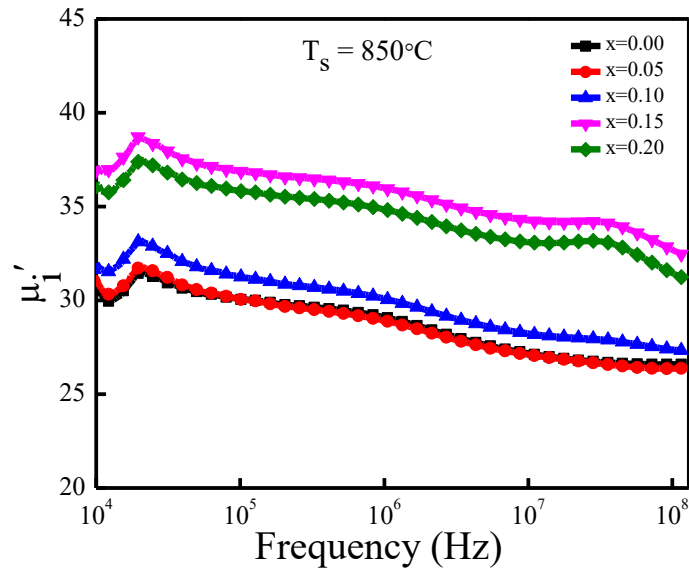
Thus the conduction process in the present composition is mainly due to small polaron hopping. According to Jonscher's law the variation of  $\log(\sigma_{ac})$  with  $\log(\omega)$  should be linear. However, a slight deviation from linearity is attributed to mixed polaron (small/large) conduction. Hopping mechanism is favored in ionic lattices in which the same kind of cation is found in two different oxidation states. Thus, in the conduction process, the hopping of 3d electrons between  $\text{Fe}^{2+}$  and  $\text{Fe}^{3+}$  might play an important role. Hopping mechanism is very useful for analyzing the conduction process in materials, for determining the activation energy and the nature of electron-phonon coupling [24].

## 4.7 Complex Initial Permeability

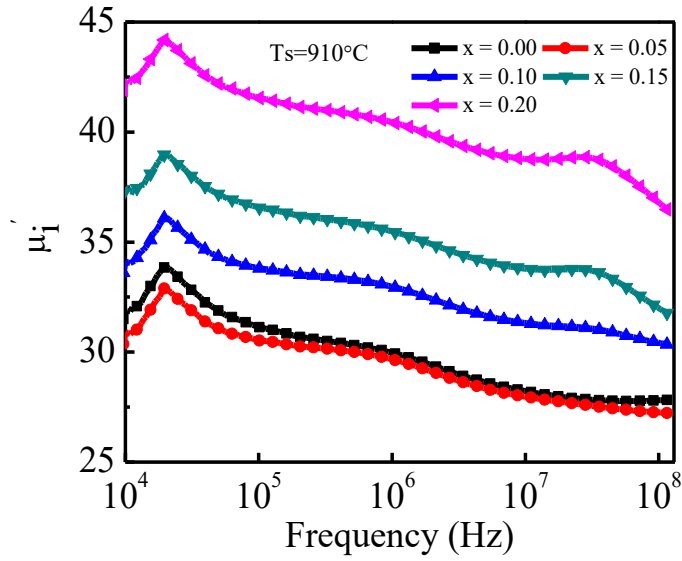
### 4.7.1 Real part of complex permeability

Fig. 4.10 shows the variation of real part of complex initial permeability ( $\mu'_i$ ) with frequency for various  $\text{Bi}_{0.9-x}\text{Ca}_{0.1}\text{Y}_x\text{Fe}_{0.9}\text{Zr}_{0.1}\text{O}_3$  compositions within the frequency range of 100 KHz-100 MHz measured at room temperature sintered at  $850^\circ\text{C}$ ,  $910^\circ\text{C}$  and  $930^\circ\text{C}$ . From figure, it

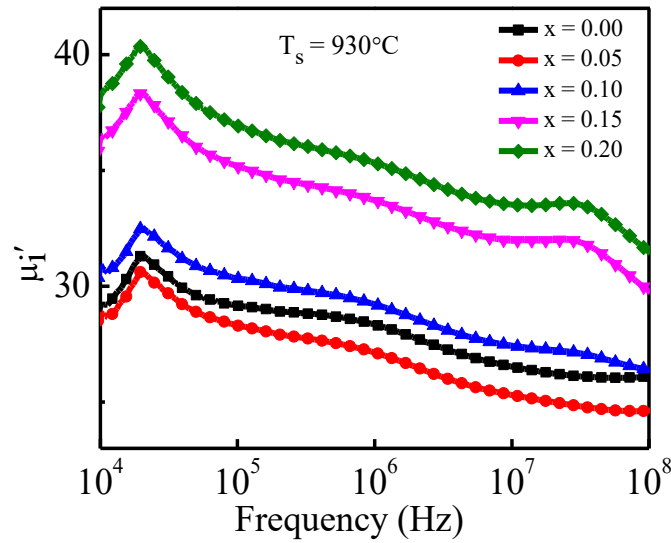
is seen that the value of real part of complex permeability for all compositions increases upto a certain frequency and then decreases with increasing in frequency. It is also observed that the value of real part of complex permeability is found 17 at 100KHz. Initial permeability in a material originates because of the spin rotation and domain wall motion. The  $\mu'_i$  decreases with frequency which is due to the fact that at higher frequencies pinning points are found to be originated at the surface of the samples from the impurities of grains and intragranular pores. This phenomenon in turn obstructs the motion of spin and domain walls and the contribution of their motion towards the increment of permeability decreases [25]. Actually it is difficult to explain compositional dependence of  $\mu'_i$  for the case of polycrystalline materials because  $\mu'_i$  depends on many factor such as stoichiometry, composition, average grain size, spin rotation, porosity, impurity, coactivity etc. In BFO, oxygen vacancies create due to the reduction of  $\text{Fe}^{3+}$  and volatilization of  $\text{Bi}^{3+}$  during sintering process. The oxygen vacancies may affect domain wall motion by the formation of mechanical barrier against the domain wall [26]. All the compositions with Y doped, sintered at 910°C and all the compositions with Y doped sintered at 930°C show that large value of permeability than all the compositions with Y doped sintered at 850°C. This may be due to the decreasing of oxygen vacancy. Permeability also depends on homogeneity of grains of a material. The materials with homogeneous grain show higher values of permeability. That is ensured from SEM of all samples.



**Fig. 4.10** Variation of real part of initial permeability with frequency of various  $\text{Bi}_{0.9x}\text{Ca}_{0.1}\text{Y}_x\text{Fe}_{0.9}\text{Zr}_{0.1}\text{O}_3$  samples sintered at  $850^\circ\text{C}$ .



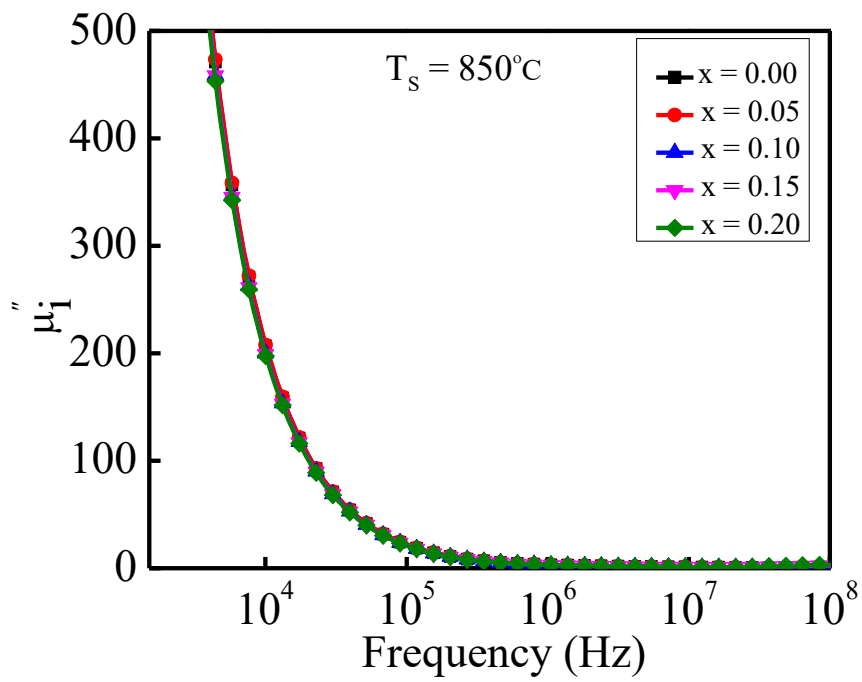
**Fig. 4.11** Variation of real part of initial permeability with frequency of various  $\text{Bi}_{0.9x}\text{Ca}_{0.1}\text{Y}_x\text{Fe}_{0.9}\text{Zr}_{0.1}\text{O}_3$  samples sintered at  $910^\circ\text{C}$ .



**Fig. 4.12** Variation of real part of initial permeability with frequency of various  $\text{Bi}_{0.9x}\text{Ca}_{0.1}\text{Y}_x\text{Fe}_{0.9}\text{Zr}_{0.1}\text{O}_3$  samples sintered at  $930^\circ\text{C}$ .

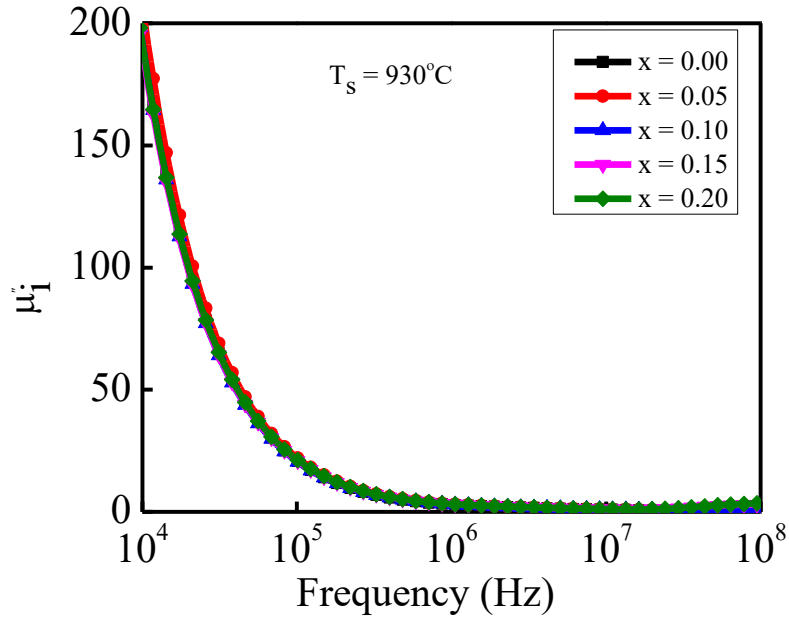
#### 4.7.2 Imaginary part of complex permeability

The frequency dependent of the imaginary part of complex permeability ( $\mu''$ ) of the composition measured at room temperature over the frequency range of 100kHz-100MHz sintered at  $850^\circ\text{C}$ ,  $910^\circ\text{C}$  and  $930^\circ\text{C}$  is shown in Fig. 4.13. In the low frequency region, the imaginary part of  $\mu''$  shows dispersion behaviors which are attributed due to domain wall displacements. Here imaginary part of  $\mu''$  decreases with increasing frequency. At higher frequency  $\mu''$  is almost independent of frequency. The  $\mu''$  is frequency independent at higher frequency region shows that there is only spin rotation is effective.



**Fig. 4.13** Variation of imaginary part of complex initial permeability with frequency of various  $\text{Bi}_{0.9-x}\text{Ca}_{0.1}\text{Y}_x\text{Fe}_{0.9}\text{Zr}_{0.1}\text{O}_3$  samples sintered at  $850^\circ\text{C}$ .

**Fig. 4.14** Variation of imaginary part of complex initial permeability with frequency of various  $\text{Bi}_{0.9-x}\text{Ca}_{0.1}\text{Y}_x\text{Fe}_{0.9}\text{Zr}_{0.1}\text{O}_3$  samples sintered at  $910^\circ\text{C}$ .



**Fig. 4.15** Variation of imaginary part of complex initial permeability with frequency of various  $\text{Bi}_{0.9-x}\text{Ca}_{0.1}\text{Y}_x\text{Fe}_{0.9}\text{Zr}_{0.1}\text{O}_3$  samples sintered at  $930^\circ\text{C}$ .

### 4.7.3 Magnetic loss

Fig. 4.16 shows that the variation of magnetic loss of various  $\text{Bi}_{0.9-x}\text{Ca}_{0.1}\text{Y}_x\text{Fe}_{0.9}\text{Zr}_{0.1}\text{O}_3$  compositions frequency sintered at  $850^\circ\text{C}$ ,  $910^\circ\text{C}$  and  $930^\circ\text{C}$ . It is seen that the value of decreases exponentially with increasing frequency. The value of remains almost constant at higher frequency. The arises due to the lag of domain wall motion with respect to applied field and creates imperfections in the lattice. The value of increases with increasing Y content due the increasing of imperfection.

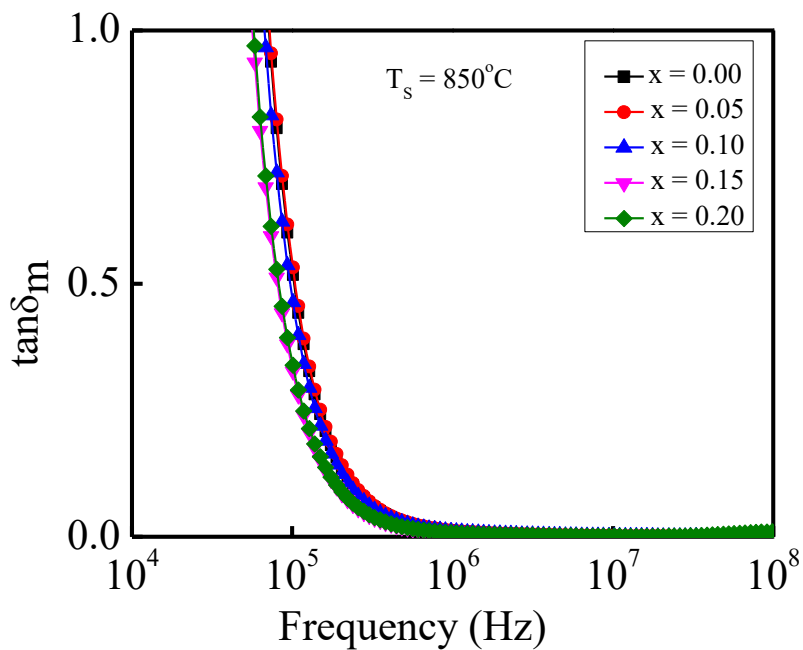


Fig. 4.16 Variation of loss factor with frequency of various  $\text{Bi}_{0.9-x}\text{Ca}_{0.1}\text{Y}_x\text{Fe}_{0.9}\text{Zr}_{0.1}\text{O}_3$  samples sintered at  $850^\circ\text{C}$ .

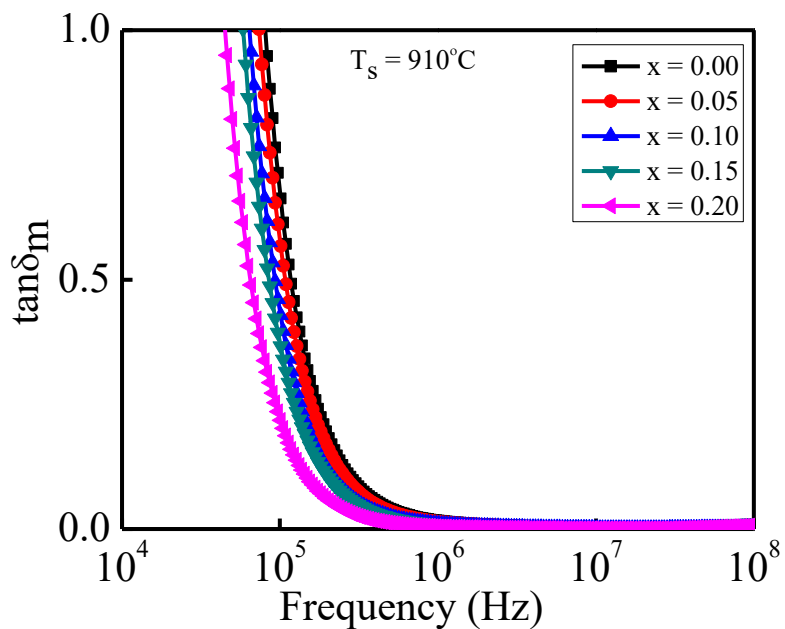
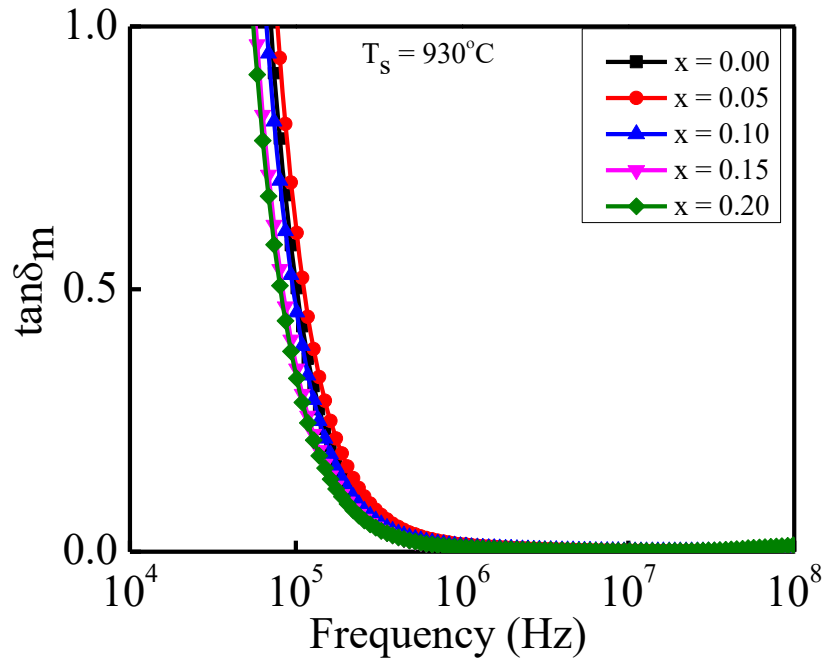


Fig. 4.17 Variation of loss factor with frequency of various  $\text{Bi}_{0.9-x}\text{Ca}_{0.1}\text{Y}_x\text{Fe}_{0.9}\text{Zr}_{0.1}\text{O}_3$  samples sintered at  $910^\circ\text{C}$ .



**Fig. 4.18** Variation of loss factor with frequency of various  $\text{Bi}_{0.9-x}\text{Ca}_{0.1}\text{Y}_x\text{Fe}_{0.9}\text{Zr}_{0.1}\text{O}_3$  samples sintered at  $930^\circ\text{C}$ .

#### 4.7.4 Relative quality factor

Fig. 4.19 shows the variation of the relative quality factor of various  $\text{Bi}_{0.9-x}\text{Ca}_{0.1}\text{Y}_x\text{Fe}_{0.9}\text{Zr}_{0.1}\text{O}_3$  samples sintered at  $850^\circ\text{C}$ ,  $910^\circ\text{C}$  and  $930^\circ\text{C}$ . It is observed that value of RQF shifts toward the higher frequency. So Y doped  $\text{Bi}_{0.9-x}\text{Ca}_{0.1}\text{Y}_x\text{Fe}_{0.9}\text{Zr}_{0.1}\text{O}_3$  materials can be used in practical applications.



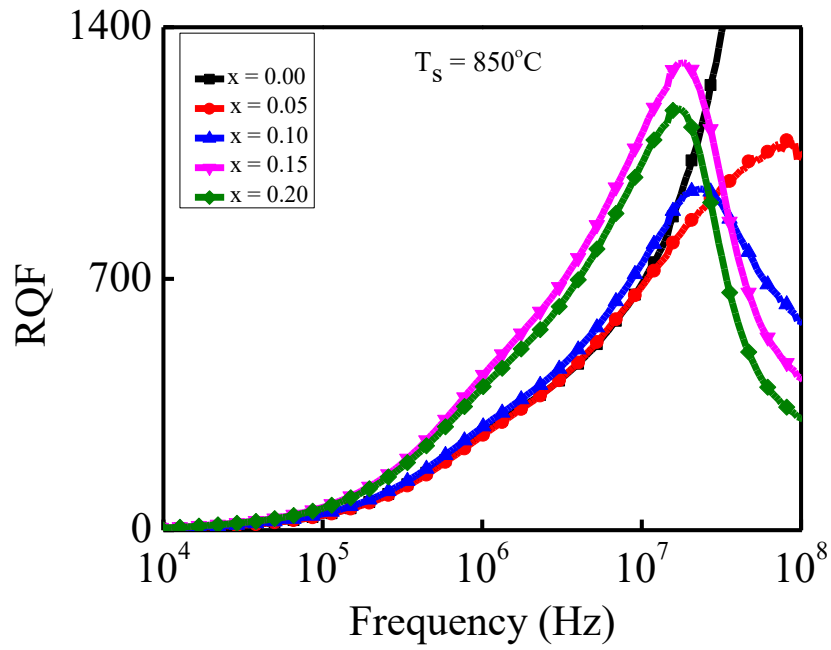


Fig. 4.19 Variation of RQF with frequency of various  $\text{Bi}_{0.9-x}\text{Ca}_{0.1}\text{Y}_x\text{Fe}_{0.9}\text{Zr}_{0.1}\text{O}_3$  samples sintered at  $850^\circ\text{C}$ .

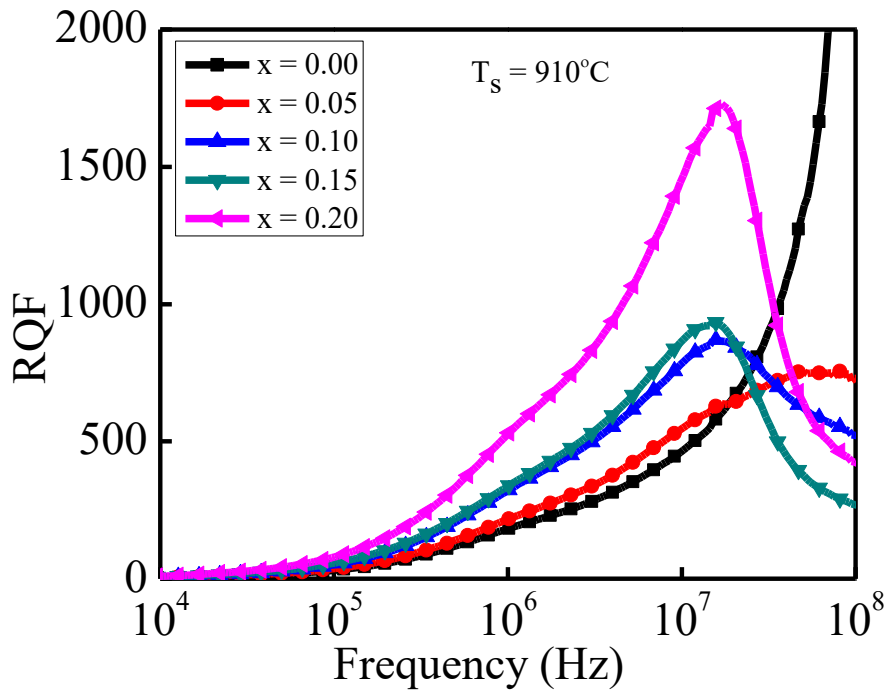
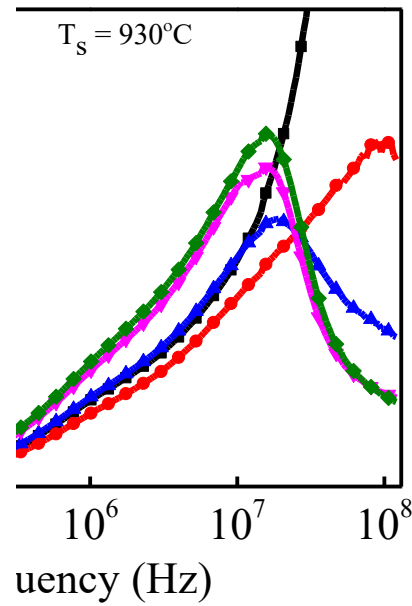


Fig. 4.20 Variation of RQF with frequency of various  $\text{Bi}_{0.9-x}\text{Ca}_{0.1}\text{Y}_x\text{Fe}_{0.9}\text{Zr}_{0.1}\text{O}_3$  samples sintered at  $910^\circ\text{C}$ .



**Fig. 4.21** Variation of RQF with frequency of various  $\text{Bi}_{0.9-x}\text{Ca}_{0.1}\text{Y}_x\text{Fe}_{0.9}\text{Zr}_{0.1}\text{O}_3$  samples sintered at  $930^\circ\text{C}$ .

#### 4.8 M-H hysteresis loops

Fig. 4.22 shows the M-H hysteresis loops of BFO (as shown in the inset) and various  $\text{Bi}_{0.9-x}\text{Ca}_{0.1}\text{Y}_x\text{Fe}_{0.9}\text{Zr}_{0.1}\text{O}_3$  ceramics. The BFO exhibits a linear magnetization as a function of the magnetic field, which is similar to earlier report [28].

Individual loops of  $\text{Bi}_{0.9-x}\text{Ca}_{0.1}\text{Y}_x\text{Fe}_{0.9}\text{Zr}_{0.1}\text{O}_3$  are shown in Fig. 4.23. In a pure  $\text{BiFeO}_3$  structure the observed net magnetization should be zero.  $\text{BiFeO}_3$  has an antiferromagnetic order but with a wavelength of 62 nm cycloid spin structure. This cycloid spin structure could be suppressed and the net magnetization will be enhanced by the uncompensated spins [27]. From Fig. 4.23, it's clear that all samples show unsaturated magnetization loops which confirm the basic antiferromagnetic nature of the compound. The magnetization increases with increasing Y content due to the structural distortion in the perovskite with change in Fe-O-Fe bond angle. This structural distortion could lead to suppression of the spin spiral and hence enhance the magnetization.

From the M – H hysteresis loops, the remanent magnetization ( $M_r$ ) was calculated using the equation:

$$M_r = \frac{|M_{r1} - M_{r2}|}{2} \quad (4.8)$$

Where,  $M_{r1}$  and  $M_{r2}$  are the magnetization with upper and lower points of intersection with  $H = 0$  respectively [31].

The coercive field ( $H_c$ ) was calculated using the equation:

$$H_c = \frac{|H_{c1} - H_{c2}|}{2} \quad (4.9)$$

Where,  $H_{c1}$  and  $H_{c2}$  are the left and right coercive field [34].

**Fig.4.22** M-H hysteresis loops of various  $\text{Bi}_{0.9-x}\text{Ca}_{0.1}\text{Y}_x\text{Fe}_{0.9}\text{Zr}_{0.1}\text{O}_3$  ceramics sintered at 910 °C.

**Fig. 4. 23** Enlarge view of the low field M-H hysteresis loops of  $\text{Bi}_{0.9-x}\text{Ca}_{0.1}\text{Y}_x\text{Fe}_{0.9}\text{Zr}_{0.1}\text{O}_3$  for  $x = 0.05$ ,  $x = 0.05$ ,  $x = 0.10$ ,  $x = 0.15$  and  $x = 0.20$

## 4.9 Magnetoelectric Coefficient

The electrical control of magnetization or magnetic control of electric polarization in the solid state is significant both fundamentally and practically. In the present case, the ME effect results from the interaction between different orderings. The ME effect in multiferroic materials arises due to interaction of the magnetic and ferroelectric domains [30]. The ME coefficient ( $\alpha_{ME}$ ) has been determined by dynamic method [31, 32] with simultaneous application of ac as well as dc magnetic field. The variation of ( $\alpha_{ME}$ ) with applied dc magnetic field for all compositions is shown in Fig. 4.24. From the figure, it is observed that  $\alpha_{ME}$  irregularly increase with increasing magnetic field for all samples. Except 0.05 composition, the value of ME coefficient gradually increases with increase of Y content. Y added samples may have improved ME coupling because of better piezoelectric properties of  $\text{Bi}_{0.9-x}\text{Ca}_{0.1}\text{Y}_x\text{Fe}_{0.9}\text{Zr}_{0.1}\text{O}_3$ . This rise in  $\alpha_{ME}$  may be attributed to the enhancement in the elastic interaction. Applied magnetic field induces large strain in magnetic domains of the samples. Due to the coupling of magnetic and ferroelectric domains the strain produces stress (strain mediated stress) in ferroelectric domains. The stress cause an increase in polarization of the ferroelectric domains and at a certain amount of Y the electric polarization becomes easier due to better piezoelectric properties as a result more bound charges to be appeared. These will help to develop more voltage in the grain which in turn produces strong ME coupling. The maximum ( $\alpha_{ME}$ ) is found to be  $230 (\mu\text{Vcm}^{-1}\text{Oe}^{-1})$  for the composition  $x = 0.20$ .

**Fig.4.24** Variation of  $\alpha_{ME}$  of various  $\text{Bi}_{0.9-x}\text{Ca}_{0.1}\text{Y}_x\text{Fe}_{0.9}\text{Zr}_{0.1}\text{O}_3$  sintered at 910°C.

## References

- [1] N.V. Minh, D.V. Thang., „Dopant effects on the structural, optical and electromagnetic properties in multiferroic  $\text{Bi}_{1-x}\text{Y}_x\text{FeO}_3$  ceramics““, *Journal of Alloys and Compounds* vol. 505 pp. 619–622, 2010.
- [2] Zhang, X., Sui, Y., Wang, X., Wang, Y., “Effect of Eu substitution on the crystal structure and Multiferroic properties of  $\text{BiFeO}_3$ ” *J. Alloys Compd.* Vol. 507 pp. 157-161, 2010.
- [3] Luo, L., Wei, W., Yuan, X., Shen, K., Xu, M., Xu, Q., “Multiferroic properties of Y-doped  $\text{BiFeO}_3$ ” *J. Alloys Compd.*, vol.540, pp. 36–38, 2012.
- [4] Case, E. D., Smyth, J. R. and Monthei, V., “Grain size determinations”, *J. Am. Ceram. Soc.*, Vol. 64, pp. C24-C25, 1981.
- [5] MacDonald, J. R., “Impedance spectroscopy”, Wiley-Interscience, New York, 1987.
- [6] Fiebig, M., Lottermoser, T. H., Fr hlich, D., Goltsev, A. V. and Pisarev, R. V., “Observation of coupled magnetic and electric domains”, *Nature*, vol. 419, pp.818-820, 2002.
- [7] J. C. Maxwell, *Electric and Magnetism*, Oxford University Press, New York, p. 828, 1973.
- [8] C. G. Koops, On the Dispersion of Resistivity and Dielectric Constant of Some Semiconductors at Audio frequencies, *Phys. Rev.* vol. 83, pp.121 – 124, 1951.
- [9] N. Rezlescu, E. Rezlescu, Dielectric properties of copper containing ferrites, *Phys. Stat. Sol. A*, vol. 23, pp 575-582, 1974.
- [10] Jonscher, A. K., “The universal dielectric response”, *Nature*, vol. 267, pp. 673-679, 1977.
- [11] Sahu, J. R., Rao, C. N. R., “Beneficial modification of the properties of multiferroic  $\text{BiFeO}_3$  by cation substitution” J. R. Sahu, C. N. R. Rao, *Solid State Sci.*, vol. 9, pp. 950-954, 2007.
- [12] Basiri, M. H., Shokrollahi, H., and Isapour, Gh., “Effects of La content on the magnetic, electric and structural properties of  $\text{BiFeO}_3$ ”, *J. Magn. Magn. Materials*, Vol. 354pp. 184–189, 2014.
- [13] Fouskova, A. and Cross, L. E., “Dielectric Properties of Bismuth Titanate”, *J. Appl. Phys.*, Vol. 41, pp. 2834, 1970.
- [14] Adler, D. and Feinlein, J., “Electrical and Optical properties of Narrow-Band Materials”, *Phys. Rev. B: Condens. Matter*, Vol. 2, pp 3112-3134, 1970.
- [15] Bauerle, E., “Study of solid electrolyte polarization by a complex admittance method”, *J. Phys. Chem.*, Vol. 30, pp. 2657-2670, 1969.
- [16] Kumar, M. M., Srinivias, A and Suryanaraybna, S. V., “Structure property relations in  $\text{BiFeO}_3$ ”

- BiTiO<sub>3</sub> solid solutions” *J. Appl. Phys.*, vol. 87, pp. 855-862, 2000.
- [17] Pattanayak, S., Chaudhury, R. N. P., Das, P. R. and Shannigrahi, S. R., Effect of Dy-substitution on structural, electrical and magnetic properties of multiferroic BiFeO<sub>3</sub> ceramics”, *Ceram. Int.*, vol. 40, pp.7983-7991, 2014.
- [18] Macedo, P.B., Moynihan, C. T. and Laberge, N. L., “The Debye-Falkenhagen theory of electrical relaxation in glass”, *Phys. Chem. Glasses*, vol. 14, pp.122, 1973.
- [19] Kaiser, M., “Electrical conductivity and complex electric modulus of titanium doped nickel-zinc ferrites”, *Physica B*, vol. 407, pp.606-613, 2012.
- [20] Choudhary, R. N. P., Pradhan, D. K., Trido, C. M. Bonilla, G. E. and Katiyar, R. S., Effect of La substitution on structural and electrical properties of Ba(Fe<sub>2/3</sub>W<sub>1/3</sub>)O<sub>3</sub> nanoceramics”, *J. Mater. Sci.*, vol. 42, pp. 7423-7423, 2017.
- [21] Pattanyak, S., Parida, B. N., Das, P. R. and Choudhary, R. N. P. “Impedance spectroscopy of Gddoped BiFeO<sub>3</sub> multiferrites”, *Appl. Phys. A*, vol. 112, pp. 387-395, 2013.
- [24] Austin, I. G. and Mott. N. F., “Polarons in crystalline and non crystalline materials”, *Adv. Phys.*, Vol. 18, pp. 41-102, 1969.
- [23] Jonscher, A. K. “The Universal dielectric response”, *Nature*, Vol. 267, pp.673-679, 1977.
- [24] Funke, K., “Jump relaxation in solid electrolytes”, *progr. Solid State Chem.*, vol.22, pp.111-195, 1993.
- [25] Globus, A., Duplex, P. and Guyot, M., “Determination of initial magnetization curve from crystallites size and effective anisotropy field”, *IEEE trans. Magn.* , Vol. 7, pp.617-622, 1971.
- [26] Das, S. R., Choudhury, R. N. P., Bhattacharya, P., Katiyar, R. S., Dutta, P., Manivannam, A. and Seehra, M. S., “Structural and multiferroic properties of La-modified BiFeO<sub>3</sub> ceramics”, *J. Appl. Phys.*, Vol. 101, pp.034104:1-4, 2007.
- [27] Anjum, G., Kumar, R., Mollah, S., Shukla, D. K., Kumar, S. and Lee, C. G., “Structural, dielectric and magnetic properties of La<sub>0.8</sub>Bi<sub>0.2</sub>Fe<sub>1-x</sub>Mn<sub>x</sub>O<sub>3</sub> (0.0≤x≤0.4) multiferroics”, *J. Appl. Phys.*, vol. 107, pp.103916, 2010.
- [28] Muthu, S. E., Singh, S., Thiyagarajan, R., Selvan, G. K., Rao, N. V. R., Raja, M. M. and Arumugam, S., “Influence of Si substitution on the structure, magnetism, exchange bias and negative magnetoresistance in Ni<sub>48</sub>Mn<sub>39</sub>Sn<sub>13</sub> Heusler alloys”, *J. Phys. D: Appl. Phys.*, vol. 46, pp.205001, 2013.
- [29] Arya, G., Kotnala, R. K. and Negi, N. S., “A Novel Approach to improve Properties of BiFeO<sub>3</sub> Nanomultiferroics”, *J. Am. Ceram. Soc.*, Vol. 97, pp. 1475-1480, 2014.
- [30] Palkar, V. R. Kundalliya, D. C. and Malik, S. K., “Magnetoelectricity at room temperature in the



- Bi<sub>0.9-x</sub>Tb<sub>x</sub>La<sub>0.1</sub>FeO<sub>3</sub> system” *Phys. Rev. B*, vol. 69, pp. 212102(1-3), 2004.
- [31] Kumar, M. M. Srinivas, A. Surayanarayan, S. V., Kumar, G. S. and Bhimasankaram, T., “ An experimental setup for dynamics measurement of magnetoelectric effect”, *Bul. Mater. Sci.*, vol. 21 pp. 251-255, 1998.
- [32] Grossiger, R., Duong. G. V. and Turtelli, R. S., “The physics of magnetoelectric composites”, *J. Magn. Mater.*, vol. 320, pp. 1972-1977, 2008.

## CHAPTER 5

### CONCLUSIONS

#### 5.1 Conclusions

The present research mainly deals with the study of structural, electrical and magnetoelectric properties of  $\text{Bi}_{0.9-x}\text{Ca}_{0.1}\text{Y}_x\text{Fe}_{0.9}\text{Zr}_{0.1}\text{O}_3$  ceramics. Disk- and toriod- shaped samples of different compositions were prepared from the synthesized powders by the solid State reaction technique and prepared samples were sintered at temperature of 850, 870, 890, 910 and 930°C as discussed in chapter 3. Number of experiments was carried out both at room temperature and at different temperatures on these samples. The results were analyzed to monitor the changes in microstructure, dielectric properties, M-H hysteresis loop, complex initial permeability and ME effect for the polycrystalline multiferroics. In this chapter a concise summary and also suggestions for the further work is presented.

The conclusions drawn from the present investigations are as follows:

Yttrium substituted various  $\text{Bi}_{0.9-x}\text{Ca}_{0.1}\text{Y}_x\text{Fe}_{0.9}\text{Zr}_{0.1}\text{O}_3$  with  $x = 0.00, 0.05, 0.10, 0.15$  and  $0.20$  were successfully synthesized by the standard solid state reaction technique. The XRD pattern indicated that polycrystalline  $\text{Bi}_{0.9-x}\text{Ca}_{0.1}\text{Y}_x\text{Fe}_{0.9}\text{Zr}_{0.1}\text{O}_3$  ceramics disclosed its crystal structure as distorted rhombohedral structure.

The value of both  $\rho_x$  and  $\rho_B$  decreased with the addition of Y in the rare earth doped-BFO. The value of  $\rho_x$  was found to be higher than that of  $\rho_B$ . Density decreased with the addition of Y content which might be attributed to the fact that the molecular weight of Bi (208.9804 g/mol) is larger than its substituted rare earth Y (88.906 g/mol).

Microstructure of the ceramics was observed by FESEM and modified with the addition of Y. The value of D was found to be increased with the increase in Y content. The percentages of elements present in various  $\text{Bi}_{0.9-x}\text{Ca}_{0.1}\text{Y}_x\text{Fe}_{0.9}\text{Zr}_{0.1}\text{O}_3$  ceramics were determined from EDX spectra. The elements present in various compositions matched well with their nominal stoichiometry which confirmed that the preparation condition completely favored the formation of the  $\text{Bi}_{0.9-x}\text{Ca}_{0.1}\text{Y}_x\text{Fe}_{0.9}\text{Zr}_{0.1}\text{O}_3$  multiferroic ceramics.

The value of  $\varepsilon'$  decreased whereas the value of also  $\tan \delta_E$  decreased with the increase in Y content and this might be attributed to the reduction of oxygen vacancies due to the addition of Y in various  $\text{Bi}_{0.9-x}\text{Ca}_{0.1}\text{Y}_x\text{Fe}_{0.9}\text{Zr}_{0.1}\text{O}_3$  ceramics. In BFO, oxygen vacancies produce during sintering process and these are responsible for the reduction of dielectric properties. It was also appeared that both  $\varepsilon'$  and  $\tan \delta_E$  decreased with increasing frequency and this might be inability of different types of polarization with the increase in frequency. The dipoles can easily follow the variation of applied field at lower frequency but at higher frequency they do not get sufficient time to align and hence cannot follow the variation of applied field; which results in the decrease of  $\varepsilon'$  and  $\tan \delta_E$ .

AC conductivity  $\sigma_{AC}$  measurement showed that  $\sigma_{AC}$  increased with the increase in frequency which implied the semiconducting behavior of the studied ceramics. Variation of  $\sigma_{AC}$  with frequency for various  $\text{Bi}_{0.9-x}\text{Ca}_{0.1}\text{Y}_x\text{Fe}_{0.9}\text{Zr}_{0.1}\text{O}_3$  ceramics followed the Jonscher's universal power law.

M-H hysteresis loop was measured for various  $\text{Bi}_{0.9-x}\text{Ca}_{0.1}\text{Y}_x\text{Fe}_{0.9}\text{Zr}_{0.1}\text{O}_3$  ceramics at room temperature and enhanced magnetization was noticed because of the addition of Y in rare earth doped BFO. The enhancement of  $M_r$  might be due to the modification of crystal structure and changing in canting angle of Fe-O-Fe.

The value of  $\mu_i'$  for various  $\text{Bi}_{0.9-x}\text{Ca}_{0.1}\text{Y}_x\text{Fe}_{0.9}\text{Zr}_{0.1}\text{O}_3$  ceramics was found to be enhanced than BFO and this might be attributed to the reduction of oxygen vacancies.  $\mu_i'$  in magnetic materials originates because of the spin rotation and domain wall motion. The oxygen vacancies may affect domain wall motion by the formation of mechanical barrier against the domain wall. Reduction of oxygen vacancies helped to facilitate the motion of domain wall and thus increased the value of  $\mu_i'$ . The values of  $\tan \delta_M$  for all the compositions decreased with frequency and addition of Y in rare earth doped BFO. The activity of domains reduced because the domains could not follow the rapid variation of the field and hence  $\tan \delta_M$  decreased at higher frequency. On the other hand,  $\tan \delta_M$  decreased with Y content because imperfection reduced with the addition of Y in BFO.

The ME coupling between the magnetic and ferroelectric order of the multiferroic  $\text{Bi}_{0.9-x}\text{Ca}_{0.1}\text{Y}_x\text{Fe}_{0.9}\text{Zr}_{0.1}\text{O}_3$  ceramics was determined by the calculation of  $\alpha_{ME}$ . The highest values of  $\alpha_{ME}$  were obtained  $230 \mu\text{Vcm}^{-1}\text{Oe}^{-1}$  for  $\text{Bi}_{0.9-x}\text{Ca}_{0.1}\text{Y}_x\text{Fe}_{0.9}\text{Zr}_{0.1}\text{O}_3$  ceramics.. The value of  $\alpha_{ME}$  was found to be enhanced than BFO which might be due to the improvement of magnetic and dielectric properties and due to the less porosity of the studied compositions.

## 5.2 Suggestions for further research

Some other investigations may be carried out on different aspects for potential applications of the studied multiferroics are given below:

- X-ray photoelectron spectroscopy (XPS) studies may be carried out to measure the oxidation states of the elements doping in the rare earth doped BFO samples.
- Transmission electron micrographs (TEM) may be taken for proper understanding of the domains.

- Neutron diffraction analysis may be performed to analyze the elemental compositions in the studied samples.
- Other preparation techniques (e.g., sol-gel, co-precipitation and auto-combustion etc.) may be followed to prepare the samples for comparing the properties of the present study.